Journal Pre-proof

The Huncal Member of the Vaca Muerta Formation, Neuquén Basin of Argentina: Insight into biostratigraphy, structure, U-Pb detrital zircon ages and provenance

Maximiliano Naipauer, Marcos Comerio, Marina A. Lescano, Verónica V. Vennari, Beatriz Aguirre-Urreta, Marcio M. Pimentel, Victor A. Ramos

Please cite this article as: Naipauer, M., Comerio, M., Lescano, M.A., Vennari, Veró.V., Aguirre-Urreta, B., Pimentel, M.M., Ramos, V.A., The Huncal Member of the Vaca Muerta Formation, Neuquén Basin of Argentina: Insight into biostratigraphy, structure, U-Pb detrital zircon ages and provenance, *Journal of South American Earth Sciences* (2020), doi: https://doi.org/10.1016/j.jsames.2020.102567.

This is a PDF file of an article that has undergone enhancements after acceptance, such as the addition of a cover page and metadata, and formatting for readability, but it is not yet the definitive version of record. This version will undergo additional copyediting, typesetting and review before it is published in its final form, but we are providing this version to give early visibility of the article. Please note that, during the production process, errors may be discovered which could affect the content, and all legal disclaimers that apply to the journal pertain.

The Huncal Member of the Vaca Muerta Formation, Neuquén Basin of Argentina: Insight into biostratigraphy, structure, U-Pb detrital zircon ages and provenance[1]

Maximiliano Naipauer[1], Marcos Comerio[2], Marina A. Lescano[3], Verónica V. Vennari[4], Beatriz Aguirre-Urreta[3], Marcio M. Pimentel[5†] and Victor A. Ramos[3]

[1] Instituto de Geocronología y Geología Isotópica, Departamento de Ciencias Geológicas, FCEN, Universidad de Buenos Aires – CONICET, Argentina. maxinaipauer@gl.fcen.uba.ar
[2] Centro de Tecnología de Recursos Minerales y Cerámica (CETMIC), Camino Centenario y 506 s/n, C.C.49 (B1897ZCA), M.B. Gonnet, Argentina (CONICET).
[3] Instituto de Estudios Andinos Don Pablo Groeber, Departamento de Ciencias Geológicas, FCEN, Universidad de Buenos Aires – CONICET, Argentina.
[4] Instituto de Evolución, Ecología Histórica y Ambiente (IDEVEA-UTN-CONICET), San Rafael, Mendoza, Argentina
[5] Institutos de Geociências, Universidade de Brasília, Brasília, Distrito Federal, Brazil.
† Deceased

Abstract. In the western sector of the Neuquén Basin, the organic-rich shales of the Vaca Muerta Formation are intercalated with turbidite sandstone intervals and slump structures integrated in the Huncal Member. The age of the Huncal sandstones based on the integration of the ammonite faunas, calcareous nannofossils and U-Pb analysis is late Berriasian in their type locality. The origin of this deposit is probably related with two lobes of turbiditic sandstones linked with a progradational regressive phase. Sandstones are lithic arkoses and feldspathic litharenites derived from recycled orogenic and dissected arc sources. The U-Pb ages confirm a mixed sedimentary provenance from the south and southeastern margins of the basin, specifically from Paleozoic and Triassic–Jurassic rocks of the North Patagonian Massif and the Huincul High. The complex fold and fault system described in the sandstone levels was interpreted as the result of slump processes with a main transport direction to the SW and W. Sandstone deposits with slump structures assignable to the Huncal Member are present throughout the entire basin from the Tithonian to the Valanginian in the Vaca Muerta Formation. Therefore, the Huncal Member is a diachronic lithostratigraphic unit and its deposition probably depended on different factors such as relative sea level changes, the position in the ramp system or in the platform and slope configuration and internal morphostructural features of the Neuquén Basin.

---

[1] *In Memoriam of Marcio Pimentel for many years of fruitful collaborative field and lab works*

1. Introduction

The lower Tithonian to lower Valanginian Vaca Muerta Formation is a complex carbonate-siliciclastic marine succession and constitutes in the last years the most analyzed hydrocarbon shale play of South American basins. It is part of the infill of the retro-arc Neuquén Basin developed at the foothills of the Andes between 34° and 40° S latitude in Argentina (Figure 1). The paleogeographic configuration of the unit shows different depositional scenarios. Towards the southern and northern regions of the basin a ramp depositional model was described from studies in outcrops (Mitchum and Uliana, 1985; Spalletti et al., 2000; Scasso et al., 2005; Kietzmann et al., 2014a), while in the subsurface of the Neuquén Embayment a platform and slope model is interpreted (Arregui, 2014; Pose et al., 2014; Gangui and Grusem, 2014; Reijenstein et al., 2017). In the western region of the basin, shale deposits are associated with turbidite sandstone levels and large subaqueous gravity slumps integrated in the Huncal Member (Leanza et al., 2002, 2003, 2011; Spalletti et al., 2008). Two opposite models have been proposed to explain the origin of the sandstones and slump structures of the Huncal Member.

Leanza et al. (2003) interpreted the sandstone levels as a turbidite succession associated with slump processes developed in the eastern platform during a highstand systems tract. However, Spalletti et al. (2008) interpreted the Huncal Member as turbidite sandstones related to large subaqueous gravity flows included in slope facies and linked with the western active margin of the basin. Although the stratigraphy, sedimentology, and bioestratigraphic features of the classical Vaca Muerta facies have been extensively studied through the years, the sandstones included in the Huncal Member have not yet been analyzed in detail. Their precise depositional age, possible correlations and extension, and if it was effectively related to a provenance from the eastern or western margin of the basin are still matters of debate.

The objective of the present work is to characterize the sandstone deposits of the Huncal Member based on sedimentological, biostratigraphic and provenance studies (i.e.: outcrop analysis, ammonite biostratigraphy, calcareous nannofossils, sandstone petrography, and U-Pb zircon ages) in order to understand the regional context and better define the provenance of the sandstones and their complex internal structure. We discuss possible correlations with other sandstone levels recorded in the Vaca Muerta Formation in several localities throughout the basin. Particularity, we discuss the

possibility to correlate the slump structures described in the Huncal Member at its type locality with other slump structures also recognized in the surface and subsurface by seismic analysis in previous works (Figure 1) (Kietzmann and Vennari, 2013; Kietzmann et al., 2014b; Arregui, 2014; Pose et al., 2014; Gangui and Grusem, 2014; Reijenstein et al., 2017). The Vaca Muerta Formation is the largest hydrocarbon source rock of Argentina and is the third reservoir in the world of unconventional gas and oil (see review in González et al., 2016), thus studies in outcrops can be very useful as possible analogues of examples recorded in the subsurface.
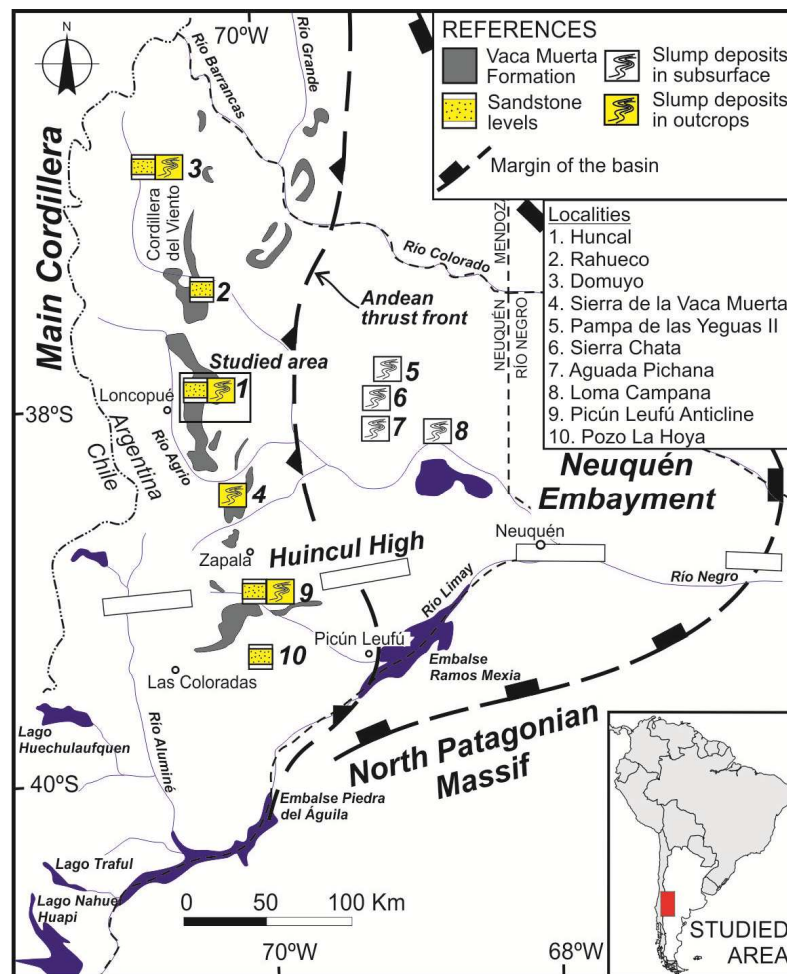

Figure 1. Regional map of the Neuquén Basin with exposures of the Vaca Muerta Formation. Localities with sandstone levels and slump type structures in outcrop sections and subsurface of the Vaca Muerta Formation are also shown. Numbers refer to localities mentioned in the text: 1) Huncal type locality (Leanza et al., 2003); 2) Rahueco (Spalletti et al., 2008); 3) Cerro Domuyo (Kietzmann and Vennari, 2013); 4) Sierra de la Vaca Muerta (Gulisano et al., 1984; Kietzmann et al., 2014b; Reijenstein et al., 2017); 5) Pampas de las Yeguas II (Gangui and Grausem, 2014; Pose et al., 2014); 6) Sierra Chata (Arregui, 2014); 7) Aguada Pichana (Pose et al., 2014); 8) Loma Campana (Reijenstein et al., 2017); 9) Picún Leufú Anticline (Krim et al., 2017); and 10) Pozo La Hoya (Santiago et al., 2014).

3

2. Geological Setting

Thick Meso-Cenozoic marine and continental successions with accurate biostratigraphic control characterize the Neuquén Basin. Many volcanic and volcaniclastic levels are exposed along its western sectors due to their retro-arc position (Digregorio et al., 1984; Ramos, 1988; Legarreta and Uliana, 1991). The stratigraphic and biostratigraphic frameworks have been studied through the years and a robust knowledge is presently available (Legarreta and Uliana, 1991, 1996; Uliana and Legarreta, 1993; Vergani et al., 1995; Aguirre-Urreta and Rawson, 1997; Aguirre-Urreta et al., 2005; and references therein).

The infill of the basin began in the Late Triassic where continental and volcanic synrift deposits were accumulated in isolated depocenters (Franzese and Spalletti, 2001). A long thermal subsidence retro-arc stage was developed between the Early Jurassic and Early Cretaceous and thick marine and continental successions with interbedded volcanogenic rocks characterized this period (Legarreta and Gulisano, 1989). Since the Late Cretaceous, the basin was filled by typical red beds deposited in a foreland basin setting (Cobbold and Rossello, 2003; Tunik et al., 2010; Fennell et al., 2017).

The Vaca Muerta Formation represents a rapid and widespread marine transgression coming from the Paleo-Pacific Ocean during the retro-arc stage of the basin according to Legarreta and Uliana (1991). The unit is composed of organic-rich black shales, marls and limestones deposited between the early Tithonian and the early Valanginian (Weaver, 1931; Legarreta and Uliana, 1991; Spalletti et al., 2000; Kietzmann et al., 2014a). The sedimentary succession is more than 800 meters thick in the main Andes of Neuquén and is widely developed in the subsurface of the Neuquén Embayment (Figure 1).

In the study area, shale-dominated distal facies of the Vaca Muerta Formation are exposed in the Agrio fold-and-thrust belt (Zamora Valcarce et al., 2006). The Huncal Member was defined by Leanza et al. (2003) in the inner zone of the belt, where turbidite sandstone intervals, in some cases with slump structures, are interbedded in the distal facies of the Vaca Muerta Formation (Figure 2).

2.1 The Huncal Member

Several localities with sandstone-dominated intervals, in cases associated with slump structures were described in the Vaca Muerta Formation (Figure 1), but there is

no agreement on the precise age of these deposits along the basin. The Huncal section is the type locality of the member (Figure 2); according to Leanza et al. (2002, 2003, 2011), the fossiliferous content of the mudstone facies, where the sandstones are interlayered, indicates an early Berriasian age for the Huncal sandstones. This relative age was based on the ammonites *Substeueroceras* sp. and *Aceveidites* sp. found 85 meters below the Huncal Member and *Argenticeras noduliferum* (Steuer) located 35 meters above it (Leanza et al., 2003). Other sandstone intervals that crop out in the Arroyo Candelero, 50 km south of the Huncal locality (Figure 2), are interbedded with fossiliferous horizons with *Berriasella callisto* (d'Orbigny) an ammonite assigned to the late Berriasian/early Valanginian by Leanza and Wiedmann (1989). The Candelero sandstones were also included in the Huncal Member by Leanza and Hugo (2005).
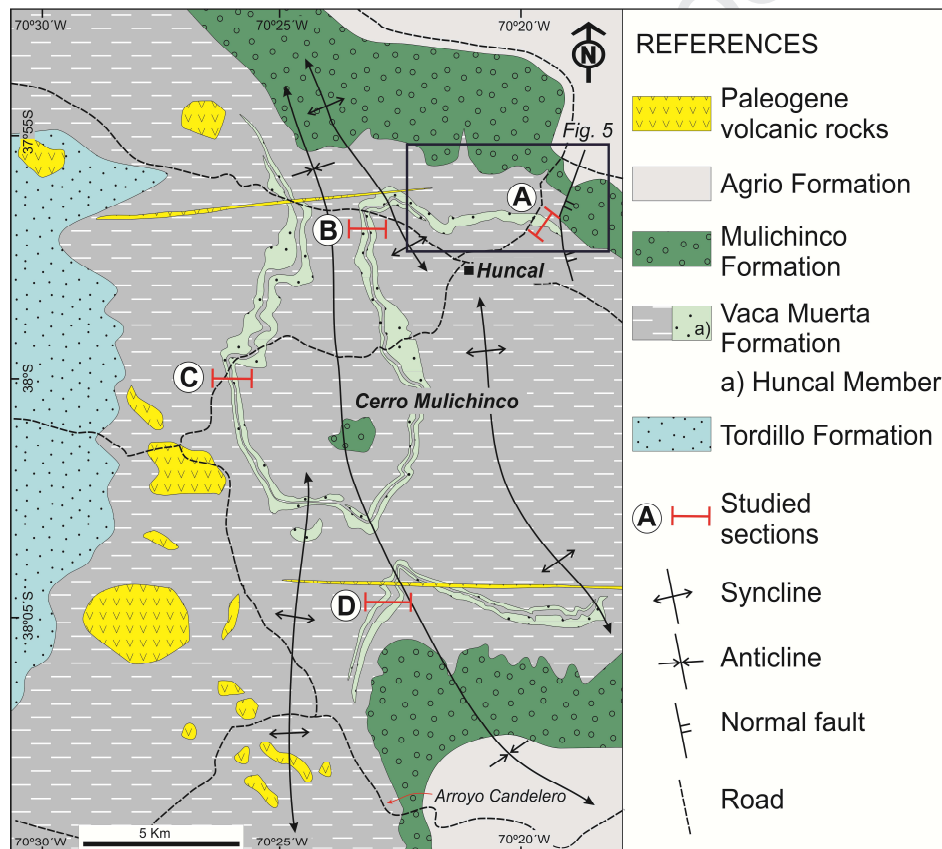
Figure 2. Geological map of the studied region based on Leanza et al. (2003, 2005, 2006), Leanza and Hugo (2005) and Zamora Valcarce et al. (2006). The studied sections and locations of Figure 3 are also shown. A) Huncal type locality (section A); B) Section B; C) section C; D) section D.

To the north of Huncal locality, in the Rahueco section (Figure 1), turbidite sandstone intervals are interbedded with mudstones of the Vaca Muerta Formation and were included in the Huncal Member by Spalletti et al. (2008). In the absence of fossils and due to their stratigraphic position, they were tentatively assigned to a late Berriasian

5

to early Valanginian age (Spalletti et al., 2008). In the area of Cerro Domuyo, located 150 km to the north of the Huncal locality (Figure 1), an interval of mudstones and calcareous sandstones with slump structures were also include in the Huncal Member (Kietzmann and Vennari, 2013; Kietzmann et al., 2014a, 2016). Their ammonite content indicates a late Tithonian age (Kietzmann and Vennari, 2013).

In the Sierra de la Vaca Muerta, 100 km to the south of the studied region (Figure 1), marls and packstones intervals with slump structures were described in the Los Catutos and Mallín de los Caballos sections (Gulisano et al., 1984; Kietzmann et al., 2014b; Reijenstein et al., 2017).

On the other hand, core samples from the La Hoya well (locality 10 in Figure 1) in the southern Neuquén Basin, show subarcosic sandstones interbedded in the typical black shales of the Vaca Muerta Formation (Santiago et al., 2014). These sandstone beds could be integrated to the Huncal Member.

Finally, complex structures interpreted as slump have been described in the subsurface of the Neuquén Embayment (Arregui, 2014; Gangui and Grausem, 2014; Pose et al., 2014; Reijenstein et al., 2017). These slump deposits were identified both seismically as well as from well profiles in different oil fields (see Figure 1). It is important to note that they were mainly recorded in late Tithonian to early Berriasian sequences and were compared with the slump structure of the Huncal Member (Arregui, 2014; Gangui and Grusem, 2014).

3. Methods

Four sections of the Huncal Member distributed in an east-west transect (Figures 2 and 3) were analyzed in order to obtain information about depositional settings, ammonite biostratigraphy, calcareous nannofossils, sandstone petrography, and U-Pb provenance. The sections were logged in detail at 1:100 and for the estimation of thickness a tape measure was used that represent one of the most precise tool for fieldwork measures. In addition, a structural section was measured at the Huncal locality along a northeast striking section of 1,200 meters to show the vergence of the structures (Figures 2 and 4).

In the four sedimentary profiles surveyed, the ammonite levels have been recognized. They are mostly represented in the shaly facies with moderate to good preservation as impressions and only in few horizons within calcareous nodules. Only on top of the Huncal Member, the ammonites are preserved as internal molds and are

6

frequently deformed. In many horizons, it was not possible to get precise systematic identifications up to the species level. The specimens were photographed, and initial identifications were done in the field which were later corroborated using appropriate literature in the laboratory.
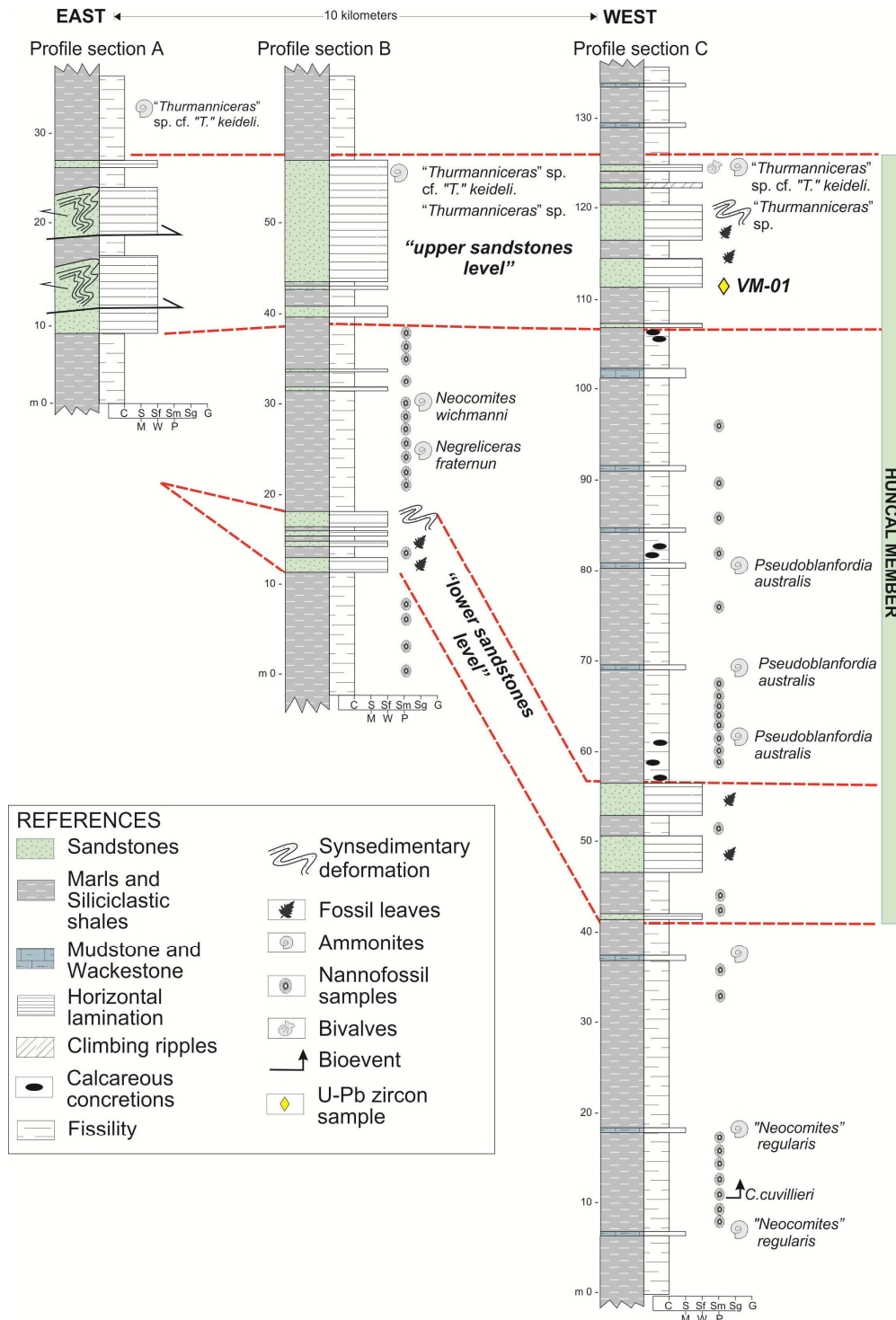

Figure 3. Measured stratigraphic profiles in an east - west transect, Huncal Member of the Vaca Muerta Formation (see location in Figure 2).

In the present study, 48 samples were analyzed for calcareous nannofossils, of which 21 were fertile. These samples are distributed as follow: in the section B (Northern profile) 16 samples were taken but only 3 were fertile, in the section C (Western profile) 14 samples were fertile of 25, and in the section D (La Silla profile) 4 samples of 7 were fertile. The micropaleontological samples were prepared following the smear slide or smear technique of Edwards (1963). The observations and photographs were made with a Leica DMLP polarization microscope with an increase of 1000X and accessories such as 1 λ plaster sheet and blue filter. The distribution charts for the calcareous nannofossil species recognized are presented in the Supplementary Material (Tables 1, 2 and 3). The material studied is deposited in the Repository of the Facultad de Ciencias Exactas y Naturales, Universidad de Buenos Aires, under the abbreviations BAFC-NP Nº: 4124 - 4139 (section B), BAFC-NP Nº: 3955 - Nº3979 (section C), and BAFC-NP Nº: 4140-4146 (section D).

Twelve standard thin sections of very fine to fine-grained sandstones of the Huncal Member were prepared and carefully analyzed under a Leica DM750P petrographic microscope fitted with a Leica MC120 HD camera. Modal composition of the different detrital grains was quantified by point counting on 300–500 points per thin section. Petrographic composition for the Huncal sandstones is presented in the Supplementary Material (Table 4).

In the upper part of the Huncal Member a fine-grained, greenish-gray sandstone was collected to analyze the detrital zircons by U-Pb laser ablation (sample VM-01, Figure 3). The zircon separation was performed by standard techniques of concentration of heavy minerals in the Departamento de Ciencias Geológicas, Universidad de Buenos Aires (Argentina). SEM (Secondary Electron Microscopy) images and U-Pb age determinations were conducted at the Laboratório de Geocronologia, Instituto de Geociências da Universidade de Brasília (Brazil). The analytical methods (LAM-MC-ICP-MS) and the age measurements of zircon grains are available in the Supplementary Material (Table 5).

4. Results

4.1. Outcrop analysis of the Huncal sections

The Huncal type locality is the most eastern outcrop (section A) and there, deformational features include several tight folds and faults that repeat and overlap various levels of sandstones and shales. Section A is between 13 and 25 meters thick

(Leanza et al., 2003; Spalletti et al., 2008) representing only the upper levels of the Huncal Member (Figures 2 and 3). Due to the high deformation, we decided to concentrate our sedimentological, biostratigraphic and provenance analysis in other sections where the sandy and shale intervals can be well distinguished (sections B, C and D). In the type locality of the Huncal Member it is more interesting to study the structural features and vergence of the deformation, which are described and analyzed in the next section.

The section B (GPS: 37º56´39.4´´S and 70º23´07.5´´W) of the Huncal Member is located west of the Huncal type locality and is 40 meters thick. The succession of the Vaca Muerta Formation here is characterized by the predominance of marls and black shales with two green, fine- to medium-grained, sandstone-dominated intervals (Figures 2 and 3). The lower sandstone-dominated interval is 7 meters thick, composed of lenticular to tabular amalgamated sandstones, ranging from 0.5 to 1.0 m thick units. Generally, sandstone beds have erosive bases and intercalate with cm-thick muddy siltstones. Sandstone beds are massive or exhibit parallel lamination and mud intraclasts represent a common feature in the base of beds. Towards the top of this interval synsedimentary structures are evident (Figure 4a). The section continues with 22 meters of shales with parallel lamination where two levels with ammonites were identified (Figure 3), the lower one carries *Negreliceras fraternun* (Steuer) and the second one *"Neocomites" wichmanni* Leanza. Above the shales, the upper sandstone-dominated interval is 17 meters thick, integrated by fine to medium-grained amalgamated massive sandstone beds. In these deposits it is common the occurrence of abundant plant debris such as leaves (Figure 4b). On its top, the third level with ammonites (*"Thurmanniceras"* sp. cf. *"T." keideli* and *"Thurmanniceras"* sp.) is registered. Along the section, 16 samples of black shales were obtained for nannofossils analysis (see below).

The section C was measured in the western flank of the Cerro Mulichinco (38º00´00.1´´S - 70º26´08.7´´W), 10 km southwest of the type locality (Figures 2 and 3). The logged section is composed of 130 meters of black shales and marls interbedded with very thin calci-mudstones and wackestones. In the lower 45 meters of the section, two thin mudstone levels record the ammonite *"Neocomites" regularis* Leanza. The Huncal Member is also characterized by two sandstone-dominated intervals separated by 50.5 meters thick shales (Figure 4c). The lower interval is 15 meters thick, while the upper one is 18 meters thick. Internally, both intervals contain tabular and lenticular

9

amalgamated massive beds, ranging from 1 to 5 meters thick (Figure 4d), in some cases with parallel lamination. Quartz and white mica are the main component in addition to mud intraclasts frequently observed towards the base of sandstone beds. High carbonaceous content and leaves characterize the deposits. In the upper interval some red sandstones show small scale synsedimentary deformation features. The shales intercalated between the two sandstone-dominated intervals record three levels with the ammonite *Pseudoblanfordia australis* (Burkhardt) well preserved in calcareous nodules. In the top of the sandstones of the upper interval, molds of deformed ammonites (*"Thurmanniceras"* sp. cf. *"T." keideli* and *"Thurmanniceras"* sp.) and bivalves are common. Along the 130 meters of the section, 25 samples of black shales were obtained for nannofossil analysis (see below).
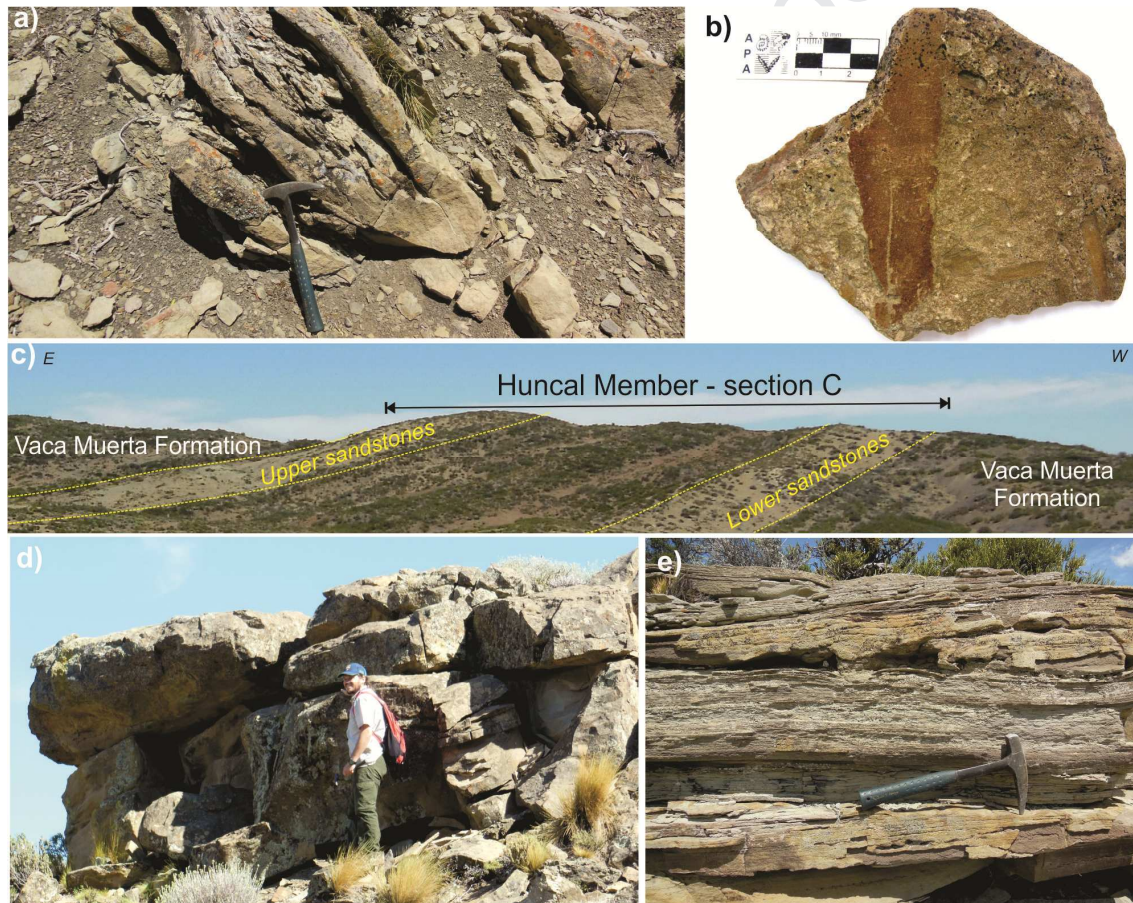
Figure 4. Photographs of the Huncal Member (Vaca Muerta Formation) outcrops; a) lower sandstone interval with synsedimentary structures at section B; b) detail of plant debris in sandstones from the Huncal Member; c) regional view of the two sandstone intervals of the Huncal Member in the section C; d) Massive sandstones with tabular and lenticular amalgamated beds; and e) sedimentary structures include horizontal lamination and low-angle lamination.

In the southern sector of the studied area, a third section was logged of the

Huncal Member (section D in Figure 2). However, as the exposures are poor, it was not possible to log it in detail. The two sandstone-dominated intervals are also recognized, being intercalated approximately by 30 meters of laminated shales. Sandstone beds are massive in some cases, but several sedimentary structures have been recognized including parallel to low-angle lamination (Figure 4e). In addition, flute casts, longitudinal scours, mud intraclasts and small scale soft-sediment deformation structures are exhibited. Many leaves were identified in the top of the sandstones; the ammonite *Pseudoblanfordia australis* (Burckhardt) was identified in lower and middle levels within the shales where seven samples were obtained for nannofossil analysis (see below).

4.1.1 Structural features in the Huncal type locality

The best developed folds and faults of the Huncal Member are exposed almost along the dirty road that goes northwards from Huncal to Pichaihue Arriba (see location in Figure 5). The exposed succession corresponds to the upper part of the Vaca Muerta section, near the tectonic contact with the Mulichinco Formation. A north-striking normal fault suppressed the uppermost levels of Vaca Muerta Formation as can be seen along the road to Pichaihue Arriba. The study section is bounded along the top and at the base by gentle dipping non-deformed black shales, which clearly show that the intense deformation is concentrated within an interval of few tens of meters.
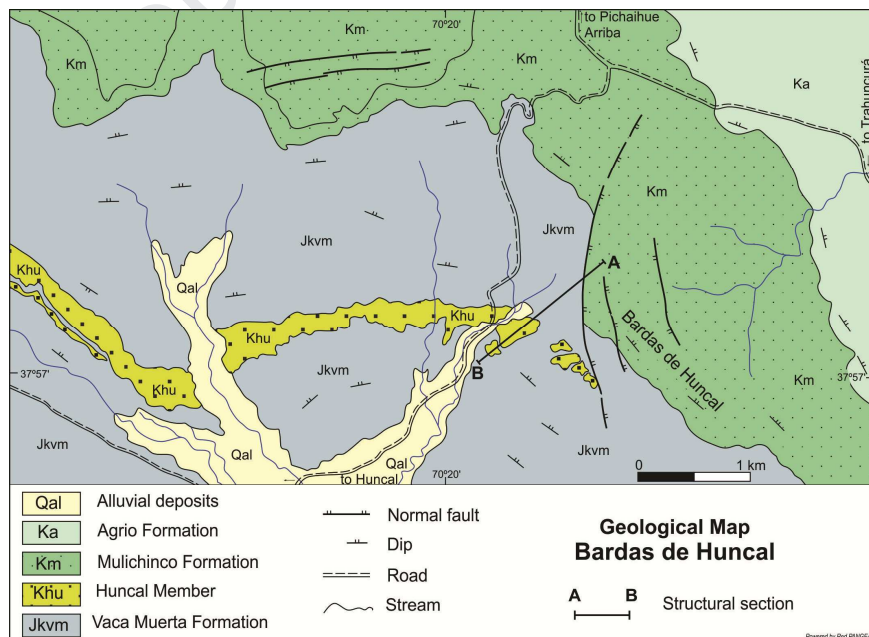
Figure 5. Detailed geological map with the location of the slump bed between A-B.

The deformed succession at Huncal is exposed along a northeast striking section

of 1,200 m. The section is described from east to west as seen in Figure 6. West of the normal fault, the upper part of the Vaca Muerta Formation is flat dipping 12ºNE. A tight anticline and a syncline are developed in the black shales, with their axial planes dipping to the east. The first yellow-greenish sandstone of 4 m thickness is interbedded in the gently folded black shales. This succession is overriding heavily deformed sandstones of the Huncal Member, in decametric folds, with their axial planes dipping to the east (Figure 6b). This deformed area is truncated by a low angle back-thrust verging N80ºE (Figure 6b). The back-thrust could be near horizontal if tilt corrected by the present Andean dip to the east of the succession.
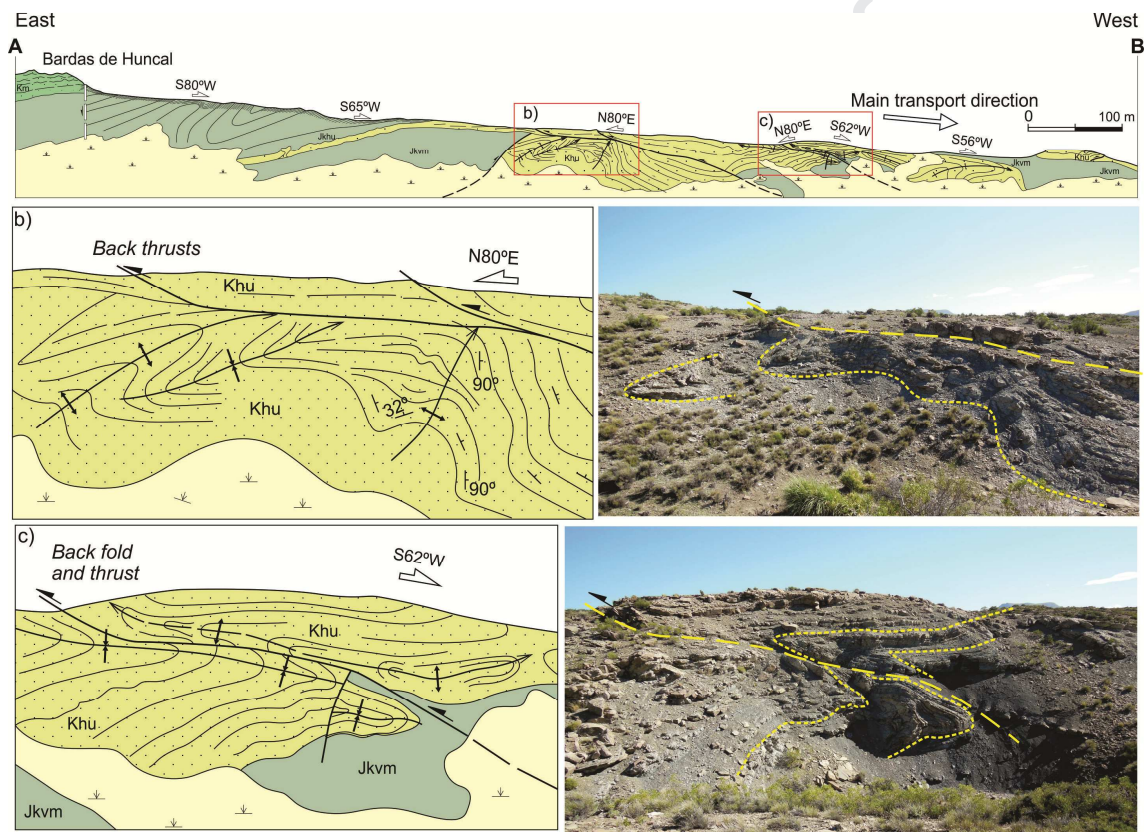
Figure 6: Cross-section of the fold and thrust system surveyed in the type locality of the Huncal Member. For location and map unit references, see Figure 5.

A second area of intense deformation is illustrated in the Figure 6c. These structures have been described by Leanza et al. (2003) and Spalletti et al. (2008). The footwall of the structure is characterized by an overturned syncline plunging 10 to 12ºW. The hanging wall structure is a double-vergent anticline, subparallel to the footwall syncline. The tectonic contact is interpreted as a back-thrust with an apparent vergence of N82ºE. However, if these structures are corrected by the Andean tilting (~ 12ºE), the axial planes of the folds are subhorizontal with a gentle dip to the north.

12

Based on this fact, the general structure is interpreted as transported in a S62ºW direction. The structure further west is characterized by another double-vergent anticline with subhorizontal axial planes, which when corrected has a gentle dipping to the east. The last isolated structures are secondary folds developed in the westernmost sector with clear west vergence.

As a whole, the described section shows some kind of chaotic structures, with apparent vergence in several directions, but with the main transport direction to the southwest. However, the vergence in some areas is very complex as shown by the orientation of the sole marks to the north and east reported by Spalletti et al. (2008), as well as some east vergence structures further to the north.

4.2. Ammonite biostratigraphy

In all the sections surveyed in this study several levels with ammonites have been identified. Representative species are illustrated in Figure 7.

In section C, within the western profile, the lowermost ammonite found is *"Neocomites" regularis* Leanza preserved in thin mudstone levels below the sandstones of the Huncal Member. The most common species recorded in the shales in between the two sandstones packages is *Pseudoblanfordia australis* (Burkhardt), an Andean endemic ammonite of late Berriasian age which was identified in the southern La Silla profile and in the western profile (sections C and D; see Figures 2 and 3). In the section B, the ammonites registered in the shales between the sandstones are *Negreliceras fraternun* (Steuer) below and *"Neocomites" wichmanni* Leanza, above. On the top surface of the Huncal Member, numerous molds of *"Thurmanniceras"* sp. and *"Thurmanniceras"* sp. cf. *"T". keideli* have been documented.

The age of this fauna is late Berriasian, representative of the *Spiticeras damesi* biozone. It should be noted here that, although *"Neocomites" wichmanni* has been considered an index species of early Valanginian age, its precise systematic position and age are presently under study.

Other ammonite species have been described and illustrated from the upper part of the Vaca Muerta Formation in a locality 8 km to the southwest of Huncal (very close to our section C) by Leanza and Wiedmann (1989). These correspond to *Thurmanniceras huncalense* and *Killianella primaeva* Leanza and Wiedmann spp. and *Protancyloceras* sp. and were recorded in the *Spiticeras damesi* zone of the late Berriasian.

13
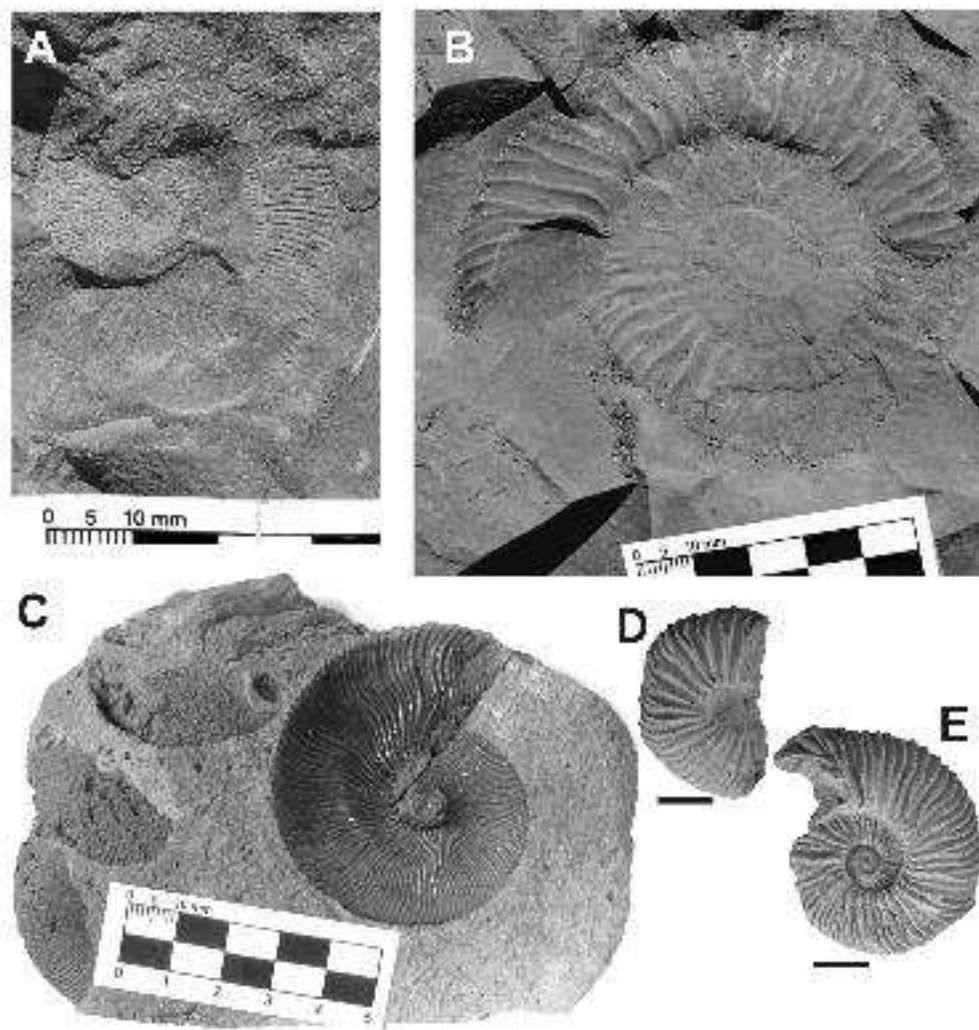
Figure 7. Field photographs of ammonites of the Huncal Member. A) *"Neocomites" regularis* Leanza, B) *Pseudoblanfordia australis* (Burckhardt), C) *"Neocomites" wichmanni* Leanza, D-E) "*Thurmanniceras*" sp. cf. *"T." keideli*. A, B, D and E from section C, C from section B. Scale bar 1 cm.

4.3. Calcareous nannofossils: bioevents and paleoecological indicators

In the section C, 21 species of calcareous nannofossil assignable to the Berriasian have been recognized with a moderate diversity and preservation. The taxa examined are *Cruciellipsis cuvillieri* (Manivit) Thierstein, *Cyclagelosphaera margerelli* Noël, *Diazomatolithus lehmanii* Nöel, *Eiffellithus primus* Applegate and Bergen, *Ethmorhabdus gallicus* Noël, *Ethmorhabdus hauterivianus* (Black) Applegate *et al. (1989), Helenea chiastia* Worsley, *Manivitella pemmatoidea* (Deflandre) Thierstein, *Micrantholithus hoschulzii* (Reinhardt) Thierstein, *Micrantholithus obtusus* Stradner, *Micrantholithus* sp.*, Retecapsa surirella* (Deflandre and Fert) Grün, *Rhagodiscus asper* (Stradner) Reinhardt, *Staurolitites* sp., *Tegumentum stradneri* Thierstein, *Tranolithus*

14

gabalus Stover, *Umbria granulosa* Bralower and Thierstein, *Watznaueria barnesiae* (Black) Perch-Nielsen, *Watznaueria biporta* Bukry, *Watznaueria fossacincta* (Black) Bown, *Zeugrhabdotus embergeri* (Noël) Perch-Nielsen, *Zeugrhabdotus howei* Bown, *Zeugrhabdotus xenotus* (Stover) Burnett. Representative species are illustrated in Figure 8.

Four biomarker species are recognized: *Umbria granulosa*, *Eiffellithus primus*, *Rhagodiscus asper* and *Cruciellipsis cuvillieri* which first occurrences (FO) are defined in the Tethys as close to the Jurassic/Cretaceous boundary. In this study, based on the joint presence of these species and in particular the FO of *Cruciellipsis cuvillieri* recognized in the basal profile levels (BAFC-NP 3957) a Berriasian age is assigned to the nannoflora recognized in the western profile (Bralower et al., 1989; Ogg et al., 2004). The absence of species of the genus *Nannoconus* Kampter prevents refining the age of this nannoflora within the Berriasian. In the Neuquén Basin, the FO of *C. cuvillieri* has been correlated, with doubts, with the *Argentiniceras noduliferum* ammonite biozone (Aguirre-Urreta et al., 2005) but its presence has been used in different regions of the basin as a Berriasian *sensu lato* biomarker (Gatto, 2007; Lescano and Concheyro, 2014).

Only few nannofossil genera have been found in the section C, but some present paleoecological relevance. Species of the genera *Watznaueria* Reinhardt and *Micrantholithus* Deflandre constitute more than 90% of the recognized taxa. *Watznaueria* spp. (*W. fossacincta*, *W. barnesiae*, *W. biporta*) is the most abundant group in all the samples. These species are considered resistant to diagenesis (Roth and Krumbach, 1986; Premoli-Silva et al., 1989; Williams and Bralower, 1995; Pittet and Mattioli, 2002) and are defined as ecologically robust forms that constitute the first species to be established in new biotopes (Mutterlose, 1991).

In oceanic environments *Watznaueria barnesiae* presents peaks in its abundance in oligotrophic conditions, whereas in restricted basins, as can be considered the "Western Interior" (USA) the peaks of *Watznueria barnesiae* are recorded in eutrophic environments (Cobianchi, 2002; Lees et al., 2004). These restricted basins are considered to have a higher nutrient level than the ocean, and runoff plays a very important role. In this study, *W. fossacincta* is more common in most samples than *W. barnesiae*, while *W. biporta* is rare (see range chart in supplementary material).
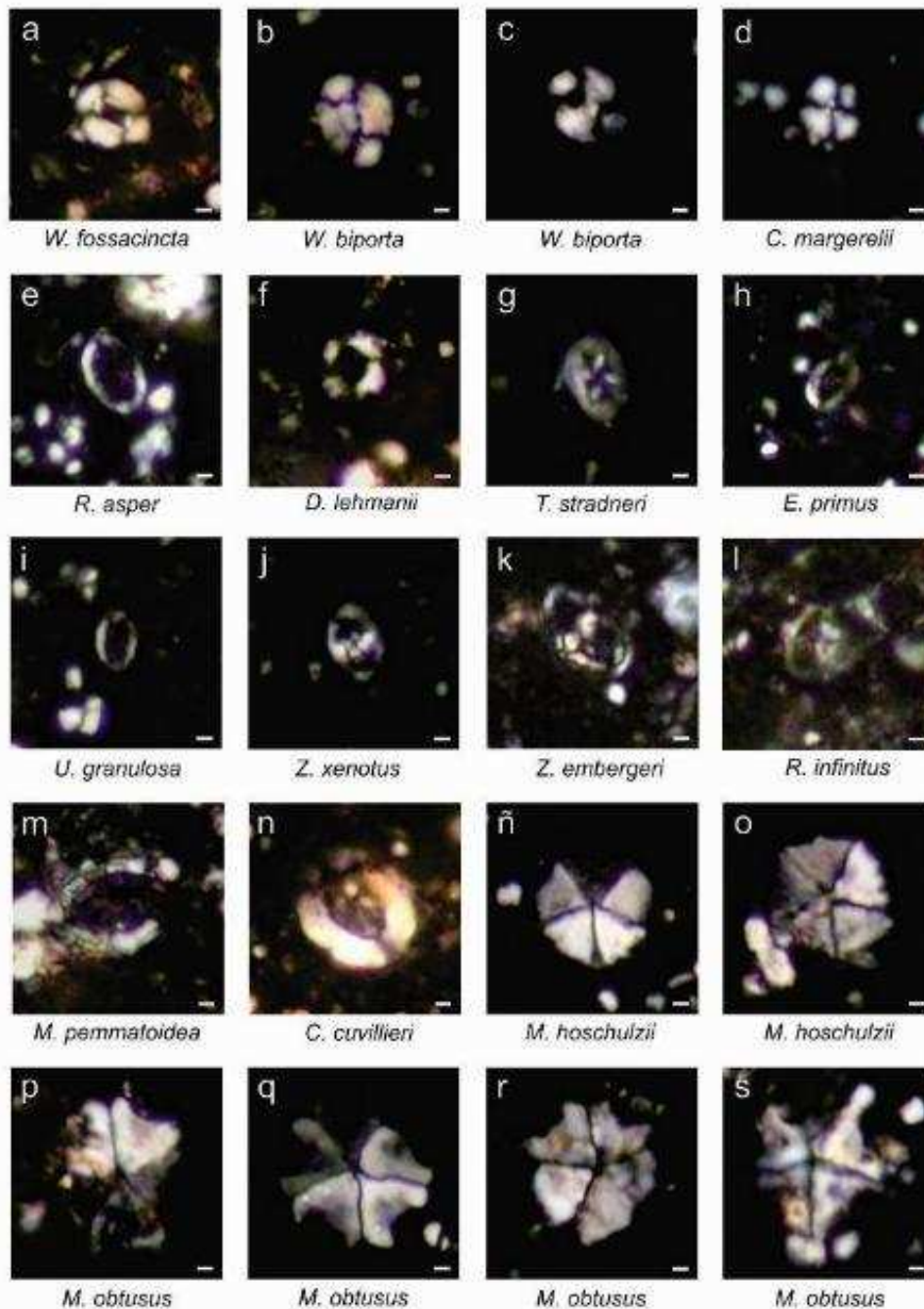
Figure 8. Representative calcareous nannofossils from the Vaca Muerta Formation at the section C (western profile). a. *Watznaueria fossacincta* (Black) Bown; b-c. *Watznaueria biporta* Bukry; d. *Cyclagelosphaera margerelii* Noël; e. *Rhagodiscus asper* (Stradner) Reinhardt; f. *Diazomatolithus lehmanii* Noël; g. *Tegumentum stradneri* Thierstein; h. *Eiffellithus primus* Applegate and Bergen; i. *Umbria granulosa* Bralower and Thierstein; j. *Zeugrhabdotus xenotus* (Stover) Burnett; k. *Zeugrhabdotus embergeri* (Noël) Perch-Nielsen; l. *Rhagodiscus infinitus* (Worsley) Applegate; m. *Manivitella pemmatoidea* (Deflandre) Thierstein; n. *Cruciellipsis cuvillieri* (Manivit) Thierstein; ñ-o. *Micrantholithus hoschulzii* (Reinhardt) Thierstein; p-s. *Micrantholithus obtusus* Stradner. Scale bar = 1 µm.

16

Micrantholithus spp. (*Micrantholithus* sp., *M. hozchulzii*, *M. obtusus*) represent the second most common group in the analyzed samples. *Micrantholithus* is interpreted as a taxon of warm waters and appears to have had a neritic distribution with a broad latitudinal range between 50ºN – 50ºS. Species are common in coastal environments and infrequent in pelagic environments (Applegate et al., 1989; Street and Bown, 2000). *Micrantholithus* is virtually absent in the Pacific and Indian oceans (Bown, 2005). Based on its similarities with the extant *Braarudosphaera bigelowi*, the ecology of *Micrantholithus* is probably related to neritic factors such as reduced salinity (Street and Bown, 2000; Bown, 2005). In addition, during the Cretaceous, the peaks in abundance of this genus are associated with low salinity values of surface waters. The increase in the abundance of *Micrantholithus* is associated with hypohaline conditions linked with the entry of freshwater flows in hotter and more humid conditions (Bersezio et al., 2002).

Another species with recognized paleoecological value is *Rhagodiscus asper*. This is a characteristic taxon of warm waters (Erba, 1987; Mutterlose, 1992; Erba et al., 1992; Street and Bown, 2000; Melinte and Mutterlose, 2001; Herrle et al., 2003; Mutterlose et al., 2005).

In the fossil record, the genus *Nannoconus* has been interpreted as an indicator of the lower part of the photic zone (Erba, 1994; Coccioni et al., 1992; Bersezio et al., 2002) and the changes registered in the abundance of the nannoconids and other nannoliths have been used to reconstruct the fertility of surface waters and to characterize the dynamics of nutrition. In the intervals in which the water presented a greater stratification, a high abundance of nannoconids would be observed accompanied by a decrease in the number of other nannofossils, and from this situation an increase in the productivity of the lower part of the photic zone is inferred (Erba, 2004). In addition, it has also been observed that a rise in nutrition (associated, for example, with an increase in seasonal winds) would generate a greater transfer of nutrients to surface waters. This would be reflected in an increase in the abundance of nannofossils and a decrease in the number of nannoconids (Erba, 2004).

In sections B and D the calcareous nannofossil assemblages recognized show moderate diversity and preservation (Tables 2 and 3 of the Supplementary Material). The nannofossil markers have not been found and therefore it has not been possible to identify a precise age for this interval.

17

4.4. Provenance analysis

4.4.1. Sandstone petrography

Modal composition of the detrital grains is plotted in the sandstone classification diagram of Folk et al. (1970), being classified as lithic arkose and feldspathic litharenite (Figure 9a). According to compositional QFL and QmFLt provenance triangles (Dickinson et al., 1983; Dickinson, 1985) sandstone samples plot near the boundary between the mixed (recycled orogenic) and dissected arc provenance fields (Figure 9b and c). Petrographic analysis indicates that the coarser grained sandstones typically tend to be better sorted than the finer grained sediments which in some cases are poorly sorted. The grain shape is mainly subangular, but well-rounded grains are also found; additionally, grain contacts are point-shaped to elongated (Figure 9d). Detrital quartz (29–46 vol.%) is mainly monocrystalline and, less commonly, polycrystalline grains show granoblastic and microcrystalline textures (Figures 9d and e). Detrital feldspars (21–34 vol.%) are dominated by plagioclases (oligoclase - andesine) but also include alkali feldspars, represented by orthoclase, and in lower proportion, sanidine and microcline are also present (Figure 9e). In general, feldspars are corroded; plagioclases show dissolution features being partially replaced by spar calcite, while alkali feldspars are incipiently altered to illite/mica. The rock debris (13–26 vol.%) are dominated by volcanic rock fragments exhibiting felsitic, hyaloplitic, and pilotaxitic textures. In minor proportion (<5% vol.%) there are also mica-rich metamorphic and plutonic rock fragments as well as illite-rich sedimentary lithics. The latter are deformed among more rigid crystal grains and form part of a pseudomatrix (e.g., Worden and Morad, 2003).
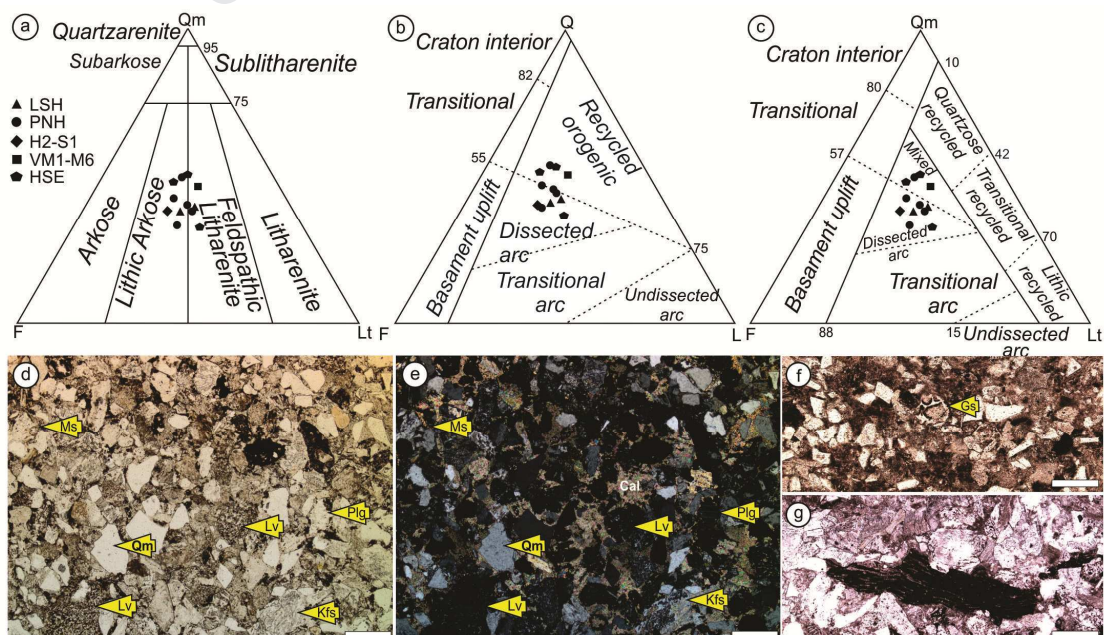
Figure 9. Petrographic characterization of the Huncal Member sandstones. a) Modal composition (QmFLt) according to the classification diagram of Folk et al. (1970); b and c) Provenance QFL and QmFLt triangles after Dickinson et al. (1983); d and e) Optical photomicrographs under parallel and crossed nicols respectively. Representative example with major framework grains: Qm (monocrystalline quartz), Plg (Ca-Na feldspars), Kfs (K-Na feldspars), Lv (volcanic lithic), Ms (muscovite); f and g) Detail microphotographs showing glass shard (Gs) with remnants of bubble walls in (f); and, organic particles that represents land-derived plant fragments in (g), both pictures taken under parallel nicols. Scale bars: 200μm in d, e and g; and 100μm in f.

The matrix is composed of phyllosilicates (mainly illite/mica and minor chlorite) and silt-sized quartz grains. Due to the similar composition between sedimentary lithics and the matrix it is possible that illite-rich lithics represent shaly intraclasts derived from the erosion of interbedded fine-grained rocks (Dickinson, 1985).

Interestingly, two samples have shown pyroclastic fragments (<1% vol.%) represented by both, glass shards and pumice fragments (Figure 9f). These components indicate that explosive volcanism processes were active during the sedimentation of the Huncal Member. Thin sections also exhibit organic particles (Figure 9g) that represent the carbonaceous particles described during fieldwork.

4.4.2. U-Pb data

Most of the separated zircons of the sample VM-01 are characterized by a long prismatic habit with an elongation greater than 3, pyramidal faces preserved and idiomorphic to subidiomorphic forms (Figure 10a). A subordinate population has rounded to subrounded forms. The SEM images of the idiomorphic to subidiomorphic zircon population showed typical oscillatory zoning indicating the igneous origin of the grains (Figure 10b). Rounded zircons presented complex internal structures suggesting a metamorphic origin. Also, in many of the zircon grains xenocrystal cores were observed.

Ninety-two zircons were analyzed by U-Pb but 20 analyses were rejected due to high discordance (more than 20%), large uncertainties, and/or Pb loss. The 72 concordant ages are between ca. 139 Ma and 1,229 Ma. The pattern of detrital zircon ages has a multimodal distribution with main peaks in the Late Jurassic at 145 Ma (10%), in the Early-Middle Jurassic at 173 Ma and 181 Ma (35%), in the Triassic at 225 Ma (14%) and in the Permian at 278 Ma (29%). Several single ages also appear in the Early Paleozoic (11%) and Late Mesoproterozoic (1%) (Figure 10 c).

The weighted average of the three youngest ages overlapping their error on one-

sigma is 144.8 ± 3.6 Ma; this value is coherent with the youngest peak in the total probability diagram at ca. 145 Ma (Figures 10 c and d).
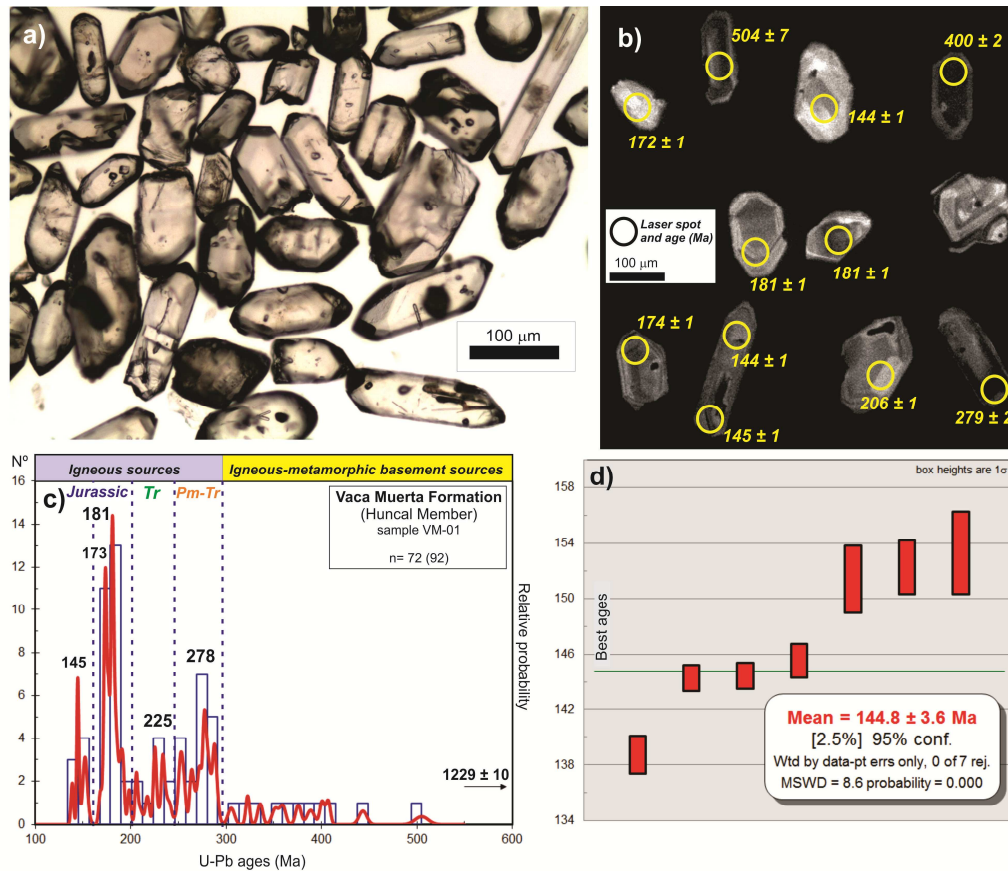
Figure 10. Microscope (a) and SEM images (b) of the analyzed detrital zircons from the VM-1 sample, Huncal Member. In the SEM images are included the laser spot positions and their age. Frequency histogram and relative probability plots of the analyzed zircons are shown in (c). Weighted average of the 3 youngest ages overlapping their error on one sigma is added in (d).

5. Discussion

5.1. Origen and age of the Huncal Member

The Huncal sandstone is a particular facies among the most common shale, mudstone and carbonate facies of the Vaca Muerta Formation. The sandstones in the type locality contain sets of sedimentary structures that allowed previous contributions to interpreting them as turbidite deposits (Leanza et al., 2003; Spalletti et al., 2008). They include massive sandstones that show flutes and small scale soft-sediment deformation features followed by fine-grained sandstones with parallel to low-angle laminated beds (Figure 4e). These vertical changes fit with models of turbidites (e.g., Bouma, 1963; Lowe, 1982; Mutti et al., 1999; Talling et al., 2012), and as observed to the north of the studied localities, fining-upward cycles were interpreted as the record of

repeated emplacement of short-lived turbidity flows (Spalletti et al., 2008). Moreover, other authors recognized combined-flow structures such as hummocky cross-stratification (Leanza et al., 2003). Also important is the abundance of plant fragments, recognized in outcrop descriptions as well as under microscopic analysis (Figures 4b, 9g).

In the western profiles two sandstone packages were recognized, which are separated by shales of variable thickness (Figure 3). The lower sandstone package disappears near the Huncal locality, while the upper level continues a few kilometers to the east. Therefore, it is possible to interpret that two independent turbiditic lobes were involved in the sedimentation of the Huncal Member.

The ammonites, mostly represented in the shaly facies between the sandstone intervals, are representative of the *Spiticeras damesi* biozone. The age assigned to the Huncal Member according to this ammonite fauna is late Berriasian. Despite the moderate diversity and preservation of the calcareous nannofossils recognized in the shaly facies of the Huncal Member, a Berriasian age is assigned to the nannoflora recognized, due to the first occurrence of *Cruciellipsis cuvillieri* documented 30 meters below of the first sandstone interval of the section C (see Figure 3). The peak of youngest U-Pb ages at ca. 145 Ma, compatible with the weighted average of the 3 youngest ages overlapping their error on 1 sigma (144.8 ± 3.6 Ma), is the best value to represent the maximum depositional age of the Huncal Member. However, this value is older than the late Berriasian age based on the biostratigraphic data. We interpret that these youngest zircons (ca.145 Ma) were recycled from the Tordillo Formation or from volcanic sources older than the sediments of Huncal Member. In addition, we conclude that the contribution of primary volcanic zircons from a volcanism coeval with the sedimentation has been no significant in the sampled level.

According to the new sequence stratigraphic framework for the Vaca Muerta Formation (Kietzmann et al., 2014a, 2016), the upper Berriasian Huncal sandstones can be included in the progradational regressive phase of the fourth transgressive-regressive composite sequence. Thus, the deposition of the turbidite sandstones at Huncal could be linked with the late stages of a prograding wedge that developed in response to relative sea-level changes. In addition, the increase in abundance of the nannofossil genus Micrantholithus in the shales recorded between the two sandstone packages, suggests changes in salinity, which could be associated with marginal environments affected by the entry of fresh water. These observations can also explain why the genus

Nannoconus has not been registered in the studied Huncal sections, but it has been recognized in more basinal localities, under normal marine conditions as Las Loicas in southern Mendoza (see Vennari et al., 2014).

5.2. Sedimentary provenance

Lower Jurassic and Permian igneous rocks were the main source area of sediment supply according to the obtained ages on the detrital zircons from the Huncal sandstones. Subordinate detrital zircon age groups in the Late Jurassic, Late Triassic and Paleozoic, plus single ages from the Early Cretaceous and Mesoproterozoic.

The best candidate to be the source region of provenance of the older detrital zircons (Lower Jurassic, Triassic, Paleozoic and Precambrian) is the North Patagonian Massif, located in the southern and eastern margin of the Neuquén Basin (Figure 11). The main group composed by volcanic zircons of the Lower Jurassic (main peak at ca. 181 Ma; 35%) could be related to volcanic rocks of the Marifíl Formation and equivalents (see Naipauer et al., 2018). The Permian detrital zircons (main peak at ca. 278 Ma; 29%) reflect a sediment supply from the western and central part of the North Patagonian Massif where Permian igneous rocks are widely distributed (e.g.: La Esperanza Plutonic Complex and Dos Lomas Volcanic Complex; see Naipauer and Ramos, 2016 for a review). The isolated early Paleozoic and Precambrian oldest ages suggest a provenance from rocks exposed in the eastern border of the North Patagonian Massif, where Lower Paleozoic igneous-metamorphic rocks are described in the Tardugno Granodiorite and the Nahuel Niyeu and El Jagüelito formations (Pankhurst et al., 2006, 2014) (Figure 11).

This interpretation is coherent with the fact that petrography of sandstones in the ternary graphs (QmFLt, QtFL, Dickinson et al., 1983; Dickinson, 1985) indicates mixed (recycled orogenic) and dissected arc provenances (Figures 9b and c). Acidic and intermediate volcanic rock fragments are the main component of lithics as was also observed by Marchese (1971), while metamorphic rock fragments are subordinate, mainly represented by polycrystalline quartz. The phyllosilicate assemblage is dominated by detrital illita/mica and minor chlorite that suggests low to medium grade metamorphic rocks as other source rocks. Therefore, the detrital components of the Huncal sandstones could have been supplied from North Patagonian Massif rocks and not significantly from the contemporary volcanic arc.

Our interpretation that the main source region for the clastic sediments was

located towards the southeast of the basin is supported by the regional depositional dip as well as the progradation of clinoforms defined by seismic interpretation in the Vaca Muerta Formation to the northwest (e.g. Gulisano et al., 1984; Legarreta and Uliana, 1991; Kietzmann et al., 2014a; Reijenstein et al., 2017).

On the other hand, the youngest detrital zircon ages (ca. 145 Ma) are more difficult to explain from the southeastern margin of the Neuquén Basin because rocks with those ages are absent in the North Patagonian Massif. The zircon group of the Late Jurassic (peak at ca. 145 Ma) should be a recycling of the underlying Tordillo Formation, as this unit has a typical most prominent peak at ca. 144 Ma (Naipauer et al., 2012, 2015). In that sense, geochemical studies conducted by Spalletti et al. (2014) also demonstrate the participation of the detritus from the Tordillo Formation in the sedimentation of the Vaca Muerta Formation during the transgressive process.

The Tordillo Formation could have been exhumed during the Early Cretaceous along the Huincul deformation zone (Naipauer et al., 2012). The Huincul High is an east-west oriented morphostructural feature that extends at depth for hundreds of kilometers across the southern Neuquén Basin (Figures 11). Several works have demonstrated a complex compressive system developed along the Huincul deformation zone and its tectonic activity during the Middle Jurassic to the Late Cretaceous (Freije et al., 2002; Mosquera and Ramos, 2006; Pángaro et al., 2009; Naipauer et al., 2012; Gangui and Grusem, 2014). This structural feature possibly constituted a positive element during the late Kimmeridgian and the Early Cretaceous (Mosquera and Ramos, 2006; Naipauer et al., 2012). Thus, the population of detrital zircon ages at ca. 145 possibly reflects a sediment supply from the Huincul High (Figure 11).

Alternatively, youngest zircons (ca. 145 Ma) could come from Late Jurassic volcanic rocks related to the Andean arc. Widely exposures of the Rio Damas Formation, located towards the northwest of the study area, are characterized by a thick volcanic sequence with U-Pb ages at ca. 146 Ma (Rossel et al., 2014) (Figure 11).

5.3. Slump structures at the Huncal locality

We interpret the complex fold and fault system described in the upper sandstone levels of the Huncal Member as the result of submarine slumps processes (Figures 5 and 6). The main features that support our interpretation are: (1) the deformed sandstone levels occur in a restricted area between undisturbed shales and (2) the structure system has a wide range of deformational style and variable vergence; although we defined a

23

main transport direction to the SW and W. In addition, the presence of these complex slump structures is not recorded westward in the studied region. In the western profiles (sections B and C) only small levels, few meters thick, show synsedimentary deformation. The distribution of the slumps is concentrated on the southern edge of the outcrops and can be recognized only in the upper sandstone levels. The lower sandstone levels of the Huncal Member disappear 5 km to the west of the type locality (section A) and were not intensely affected by slumping processes (Figures 3 and 5).
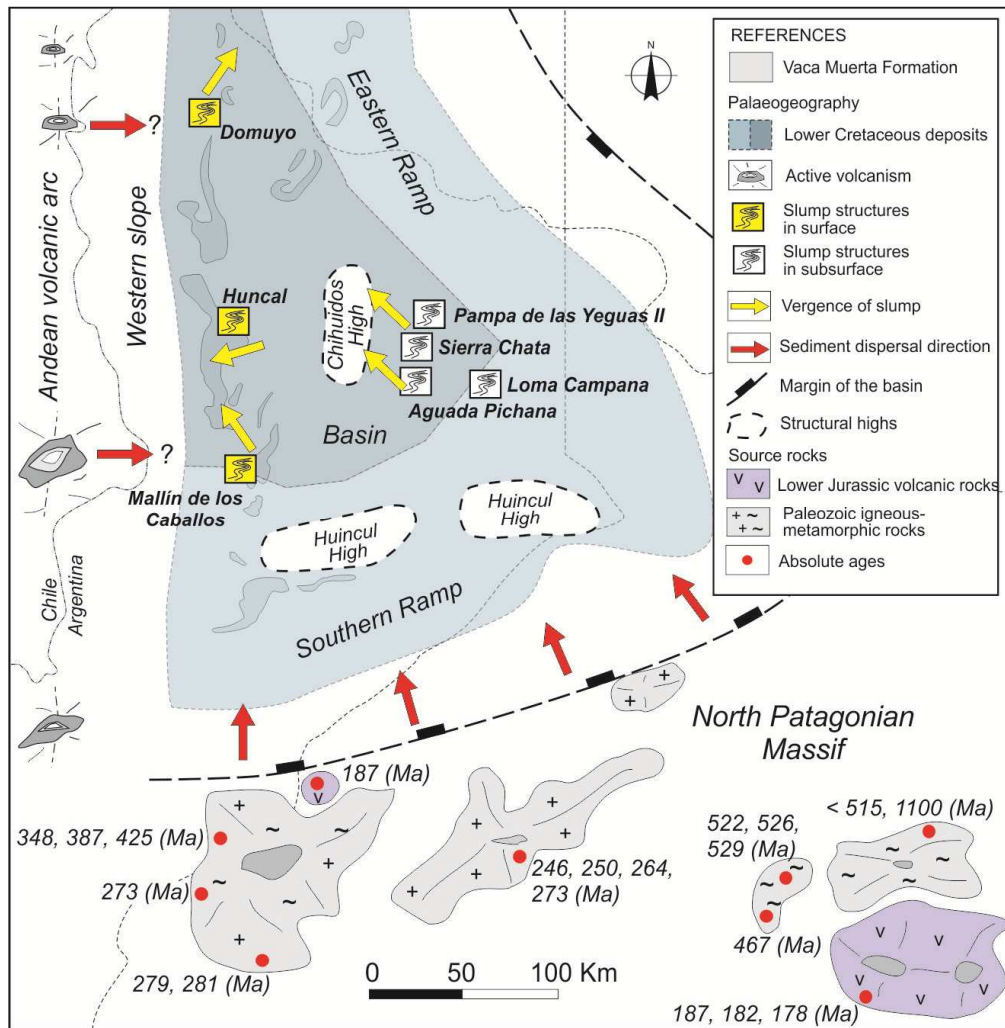
Figure 11. Simplified paleogeographic map with tectonic elements and major sediment dispersal directions for the Early Cretaceous. References of the absolute ages of the basement areas are cited in the text.

Previous works have proposed two opposite models to explain the origin of the slump structures in the Huncal Member. Leanza et al. (2003) suggested a vergence towards the NE for the slump structures (see figure 6 in Leanza et al., 2003). They highlighted that this direction is coherent with the sedimentary progradation in the inner platform setting for the Vaca Muerta Formation and its development in a highstand

24

system tract during the Berriasian (Mitchum and Uliana, 1985; Legarreta and Uliana, 1991). On the other hand, Spalletti et al. (2008) suggested that the Huncal Member represented submarine sediment deposits as a consequence of gravity-driven processes that pushed semi-lithified rocks into the mud-dominated outer ramp to basinal settings. These authors showed a main direction of transport towards the NE (see their Figure 6 b and c) based on the axial plane of the folds. However, they suggested a depositional scenario for the Huncal Member characterized by an abrupt slope zone towards the west, close to the volcanic arc.

The main slump vergence towards the SW combined with structures with opposite vergence (NE) that were interpreted as backfolds and backthrusts do not suggest an origin from the western margin of the basin (Figure 11). In addition, the sedimentary supply from sources located to the southeast, in the North Patagonian Massif, would also not agree with a simple western origin of the Huncal sandstones.

Due to the localized position of the slump, we suggest that its origin may be linked with an internal morphostructural high of the basin. The Chihuidos High, or Cerro Arenas High (according to Dominguez et al., 2017), is a subsurface structure located 50 kilometers east of Huncal (Figure 11). Its structure has undergone a differential subsidence and conforming an internal morphostructural high during the Early Cretaceous (Arregui, 2014; Dominguez et al., 2017; and references cited therein). Possible vertical movements concentrated in this structure might be the causes to destabilize previously deposited sandstones and the development of the slumping deposits in the Huncal locality.

On the other hand, the time span between the deposition of the sandstones and the generation of slump structures is controversial. There are many variables involved in the triggering process: climate-driven factors such as sea-level fluctuations and changes in sedimentation rate that impact in the pore pressure within the sediment column as well as in the hydrostatic pore water pressure. In addition to seismic shaking generated by earthquakes, among other factors (e.g. Lewis, 1971; Hampton et al., 1996; Urlab et al., 2013; Talling et al., 2012). Despite these uncertainties, the combined effect of regression during a relative fall of sea level and tectonic earthquakes due to retro-arc position of the Neuquén Basin could have promoted the instability of the deposits in the slope or ramp system of the Vaca Muerta Formation (Mitchum and Uliana, 1985; Legarreta and Uliana, 1991; Kietzmann et al., 2014a; 2016). The occurrence of tectonic earthquakes during the Late Jurassic and Early Cretaceous in the Neuquén Basin is also

supported by several soft-sediment deformation structures recorded in the base of the Vaca Muerta Formation that were attributed to a seismic origin (Martin-Chivelet et al., 2011; Kietzmann and Vennari, 2013; Gangui and Grusem, 2014).

5.4. Extension of the Huncal Member in the Neuquén Basin

It is important to note that there are several records of sandstone levels interlayered with shales in the Vaca Muerta Formation but not all of them are related to slump structures as in the Huncal locality. For instance, this is the case of the turbidite sandstones described in Rahueco by Spalletti et al. (2008) that were assigned to the upper Berriasian – lower Valanginian, and thus they could be correlated in age and lithology with the Huncal Member. Moreover, two levels of fine sandstones with leave remains were found in the Rahueco section, which support their correlation. In addition, the sandstone intervals that crop out in the Arroyo Candelero (Leanza and Hugo, 2005) can be correlated based on the late Berriasian age of the Huncal Member assigned in the present work. However, it is necessary to enhance the study of the composition and structure of these sandstones. In the Picún Leufú sub-basin, south of the Huincul High (Figure 11), Santiago et al. (2014) described two packages of massive fine sandstones between shale facies of the Vaca Muerta Formation. The study is based on the description of two core of the La Hoya well referred to the middle section of the Vaca Muerta Formation but there is not a precise temporal control. Although it is possible to establish a comparison based on the presence of the sandstone levels with the Huncal Member.

On the other hand, several deposits assigned to the Vaca Muerta Formation associated with slump structures have been registered throughout the basin. However, the age and composition of these deposits are variable (Figure 12). In the Cerro Domuyo area, an interval of approximately 60 meters of mudstones and calcareous sandstones with slump structures were included in the Huncal Member (Kietzmann and Vennari, 2013). Its ammonite content indicates a late Tithonian age, which is not in agreement with the late Berriasian age of the Huncal Member in its type locality. Another difference is the composition of the sandstones, while those from the Huncal locality are siliciclastic in composition; the sandstones from the Cerro Domuyo are calcareous.

South of the study region, in the Sierra de la Vaca Muerta (Figure 1), slump structures with NW vergence were described in marls and packstones associated with

internal and external ramp facies (Gulisano et al., 1984; Kietzmann et al., 2014b; Reijestein et al., 2017). The slump structures were related to tectonic activity in the Huincul High during the middle and late Tithonian (Kietzmann et al., 2014b). It should be noted that the composition of the slump beds of the Sierra de la Vaca Muerta locality is different from the typical sandstone facies of the Huncal Member. This difference in composition of the slump beds difficult their inclusion in the Huncal Member (Figure 12).

In the Picún Leufú Anticline, the Vaca Muerta Formation records sandstones beds associated with several slump structures assignable to the lower Tithonian (Figures 11 and 12) (Krim et al., 2017). These deposits could possibly be included in the Huncal Member taking into account their composition and structures.

Age			Ammonite Zones	Western sector				Eastern sector
				Cerro Domuyo	Study Area Huncal	Sierra de la Vaca Muerta	Picún Leufú Anticline	Neuquén Embayment (subsurface)
Early Cretaceous	Lower Valanginian		O.atherstoni	Upper Member Vaca Muerta Formation	Mulichinco Formation	Mulichinco Formation	Bajada Colorado Formation	Upper Vaca Muerta Formation
			Lissonia riverol			Quintuco Formation		
			Neocomites wichmanni					
	Upper Berr.		Spiticeras damesi		Huncal Mb.			
	Middle Berr.		Argentiniceras noduliferum		Vaca Muerta Formation	Upper Vaca Muerta Formation		Huncal Mb.
	Lower Berr.		Substeueroceras koeneni	Huncal Mb.			Picún Leufú Formation	
Late Jurassic	Upper Tithonian		Corongoceras alternans	Lower Member Vaca Muerta Fomation				
			Windhauseniceras internispinosum				Vaca Muerta Formation	
	Lower Tithonian		Aulacosphinctes proximus			Lower Vaca Muerta Formation	Huncal Mb.	Lower Vaca Muerta Formation
			Pseudolissoceras zitteli				Vaca Muerta Formation	
			Virgatosphinctes andesensis					
				Tordillo Formation				

Figure 12. Chronostratigraphic chart of the early Tithonian-early Valanginian of the Neuquén Basin with the sandstones and slump beds mentioned in the text and included in the Huncal Member (modified from Spalletti et al., 2000; Krim et al., 2017).

On the other hand, recent works in the subsurface of the Neuquén Embayment have shown very large slump structures prograding to the NW associated with the Vaca Muerta Formation (Pose et al., 2014; Gangui and Grusem, 2014; Reijenstein et al., 2017) (Figure 11). The slump structures described in the subsurface of the basin are recorded in late Tithonian – early Berriasian sequences and are include in slope facies (Arregui, 2014; Pose et al., 2014; Gangui and Grusem, 2014). The sizes of the slumps

that have been interpreted in seismic scale range from small displacements of seismic reflectors to deformed packages that extend for several kilometers and have thicknesses of up to 100 meters (Arregui, 2014; Gangui and Grusem, 2014). The smaller structures can be compared in size with the slumps described in surface of the Huncal Member. Therefore, it is also possible to include the slump beds of the subsurface in the Huncal Member (Arregui, 2014; Gangui and Grusem, 2014).

According to the above discussion, the available evidence points out that sandstones levels and slumping processes occurred recurrently from the Tithonian to the Valanginian and that they are present throughout the entire Neuquén Basin. Therefore, it should be noted that the Huncal Member is a diachronic lithostratigraphic unit. In addition, it is important to note that the vergence of the slump structures is variable and probably depends on variable factors as internal morphostructural features (e.g.: Huincul and Chihuidos highs) and position in the ramp system or in the platform-slope configuration. A common point among all of them is that the sandstones and slump are developed during a progradational regressive phase, except the slump described in the Sierra de la Vaca Muerta that is related to a transgressive systems tract (Kietzmann et al., 2014b). Therefore, the deposition of turbidite sandstones and slump structures in the Vaca Muerta Formation occurred during regressive phases probably related to episodes of relative sea-level fall (Krim et al., 2017).

6. Conclusions

The age of the Huncal Member in the type locality, based on the integration of the ammonite faunas, calcareous nannofossils and U-Pb analysis, is late Berriasian. The origin of these deposits was probably related to two lobes of turbiditic sandstones linked with a progradational regressive phase. However, a more detailed analysis of sedimentary facies must be done. The analyzed sandstones are lithic arkoses and feldspathic litharenites derived from recycled orogenic and dissected arc sources. The U-Pb ages confirm a mixed sedimentary provenance from the south and southeastern margins of the basin, specifically from Paleozoic and Triassic–Jurassic rocks of the North Patagonian Massif and the Huincul High. A contribution from the Early Cretaceous active volcanic arc in the western margin was subordinated.

The complex fold and fault system described in the upper sandstone levels of the Huncal locality was interpreted as the result of slump processes with a main transport direction to the SW and W. The combined effect of a regression during the relative fall of sea level and tectonic earthquakes due to the retro-arc position of the Neuquén Basin could have promoted the instability of previously deposited sandstones and the development of the slumps. Possible vertical movements linked with the Chihuidos High could also have triggered the instability of the sediments.

Sandstone deposits with slump beds are present throughout the entire basin from the Tithonian to the Valanginian in the Vaca Muerta Formation. Therefore, the Huncal Member is a diachronic lithostratigraphic unit and its deposition probably depended on different factors such as the relative sea level changes, the position in the ramp system or in the platform and slope configuration and internal morphostructural features of the Neuquén basin.

Finally, this study demonstrates that the combination of biostratigraphic, structural and provenance analysis provides a better understanding of a particular stratigraphic interval within the Vaca Muerta Formation, an analogy that can be used in the analysis of other source rock and unconventional units worldwide.

7. References

Aguirre-Urreta, M.B., Rawson, P.F. 1997. The ammonite sequence in the Agrio Formation (Lower Cretaceous), Neuquén Basin, Argentina. Geological Magazine 134, 449–458.

Aguirre-Urreta, M.B., Rawson, P.F., Concheyro, G.A., Bown, P.R., Ottone, E.G. 2005. Lower Cretaceous (Berriasian-Aptian) biostratigraphy of the Neuquén Basin. In: Veiga, G., Spalletti, L., Howell, J.A., Schwarz, E. (Eds.), The Neuquén Basin: A Case Study in Sequence Stratigraphy and Basin Dynamics, Geological Society of London, Special Publication 252, pp. 57–81.

Applegate, J.L., Bergen, J.A., Covington, J.M., Wise, S.W. 1989. Lower Cretaceous calcareous nannofossils from continental margin drill sites off North Carolina (DSDP Leg 93) and Portugal (ODP Leg 103): a comparison. In: Crux, J.A., van Heck, S.E. (Eds.), Nannofossils and Their Applications, Ellis Horwood, Chichester, pp. 212–222.

Arregui, C. 2014. Ciclos deposicionales de las Fms Quintuco y Vaca Muerta: génesis y evolución. Área Central – Cuenca Neuquina. 9º Congreso de Exploración y desarrollo de hidrocarburos, Trabajos Técnicos, Tomo II, 189–207.

Bersezio, R., Erba, E., Gorza, M., Riva, A. 2002. Berriasian- Aptian black shales of the Maiolica Formation (Lombardian Basin, Southern Alps, Northern Italy): local to global events. Palaeogeography, Palaeoclimatology, Palaeoecology 180, 253–275.

Bouma, A.H. 1963. Sedimentary facies model of turbidites. AAPG Bulletin 47, 351.

Bown, P.R. 2005. Early to Mid-Cretaceous Calcareous Nannoplankton from the Northwest Pacific Ocean, Leg 198, Shatsky Rise. Proceedings of the Ocean Drilling Program, Scientific Results 198, 1–82.

Bralower, T., Monechi, S., Thierstein, H. 1989. Calcareous Nannofossil Zonation of the Jurassic- Cretaceous Boundary Interval and Correlation with the Geomagnetic Polarity Timescale. Marine Micropaleontology 14, 153–235.

Cobbold, P.R., Rossello, E.A. 2003. Aptian to recent compressional deformation of the Neuquén Basin, Argentina. Marine and Petroleum Geology 20, 429–443.

Cobianchi, M. 2002. I nannofossili calcarei del Giurassico medio e superiore del bacino di Belluno (Alpi Calcaree Meridionali). Atti Ticinensi di Scienze della Terra 43, 3–24.

Coccioni, R., Erba, E., Premoli Silva, I. 1992. Barremian-Aptian calcareous plankton biostratigraphy from the Gorgo Cerbara section (Marche, central Italy) and implications for plankton evolution. Cretaceous Research 13, 517–537.

Dickinson, W.R. 1985. Interpreting provenance relations from detrital modes of sandstones. In: Zuffa, G.G. (Ed.), Provenance of Arenites, Dordrecht, D. Reidel Publishing Co., pp. 333–361.

Dickinson, W.R., Beard, L.S., Brakenridge, G.R., Erjavec, J.L., Ferguson, R.C., Inman, K.F., Knepp, R.A., Lindberg, F.A., Ryberg, P.T. 1983, Provenance of North American Phanerozoic sandstones in relation to tectonic setting: Geological Society of America, Bulletin 94, 222–235.

Digregorio, R.E., Gulisano, C.A., Gutiérrez Pleimling, A.R., Minniti, S.A. 1984. Esquema de la evolución geodinámica de la Cuenca Neuquina y sus implicancias paleogeográficas. 9° Congreso Geológico Argentino, San Carlos de Bariloche, Actas 2, 147–162.

Domínguez, R.F., Cristallini, E, Leanza, H.A. 2017. Evolución tectono-sedimentaria del sistema Vaca Muerta-Quintuco (Tithoniano a Valangianiano inferior) en el Engolfamiento Neuquino, Argentina. 10º Congreso Geológico Argentino, Simposio 5: Geología de la Formación Vaca Muerta, pp. 31-37, San Miguel de Tucumán.

Edwards, A. 1963. A preparation technique for calcareous nannoplankton. Micropaleontology 9, 103-104.

Erba, E. 1987. Mid- Cretaceous cyclic pelagic facies from the Umbrian–Marchean Basin: What do calcareous nannofossils suggest? International Nannoplankton Association Newsletter 9, 52–53.

Erba, E. 1994. Nannofossils and superplumes: The early Aptian "nannoconid crisis". Paleoceanography 9, 483–501.

Erba, E. 2004. Calcareous nannofossils and Mesozoic ocean anoxic events. Marine Micropaleontology 52, 85–106.

Erba, E., Castradori, D., Guasti, G., Ripepe, M. 1992. Calcareous nannofossils and Milankovitch cycles: the example of the Albian Gault Clay Formation (southern England). Palaeogeography, Palaeoclimatography, Palaeoecology 93, 47–69.

Fennell, L.M., Folguera, A., Naipauer, M., Gianni, G., Rojas Vera, E.A., Bottesi, G., Ramos, V.A. 2017. Cretaceous deformation of the Southern Central Andes: synorogenic growth strata in the Neuquén Group (35º 30´- 37ºS). Basin Research 29, 51–72.

Folk, R.L., Andrews, P.B., and Lewis, D.W. 1970. Detrital sedimentary rock classification and nomenclature for use in New Zealand. New Zealand Journal of Geology and Geophysics 13, 937–968.

Franzese, J.R., Spalletti, L.A. 2001. Late Triassic early Jurassic continental extension in southwestern Gondwana: tectonic segmentation and pre-break-up rifting. Journal of South American Earth Sciences 14, 257–270.

Freije, H. Azúa, G., Gonzalez, R., Ponce J., Zavala, C. 2002. Actividad tectónica sinsedimentaria en Jurásico del Sur de la Cuenca Neuquina. 5º Congreso de Exploración y Desarrollo de Hidrocarburos, Actas en CD, 17 pp., Mar del Plata.

Gangui, A., Grausem, M. 2014. Tectonismos y estilos estructurales en el engolfamiento Neuquino: implicancias en la interpretación de las fracturas monitoreadas por microsísmica en la Formación Vaca Muerta. 9º Congreso de Exploración y desarrollo de hidrocarburos, Simposio de recursos no convencionales: Ampliando el horizonte energético: 341–364.

Gatto, A.Y. 2007. Estratigrafía y estructura de la región de Los Raris, alto río Barrancas, provincia del Neuquén. Trabajo final de Licenciatura, Facultad de Ciencias Exactas y Naturales, Universidad de Buenos Aires, 108 p. Inédito.

González, G., Vallejo, D., Kietzmann, D.A., Marchal, D., Desjardins, P., González Tomassini, F., Gomez Rivarola, L., Dominguez, F. 2016. Transecta Regional de la Formación Vaca Muerta Integración de sísmica, registros de pozos, coronas y afloramientos. IAPG-AGA, 252 p.

Gulisano, C.A., Gutiérrez Pleimling, A.R., Digregorio, R.E. 1984. Análisis estratigráfico del intervalo Tithoniano-Valanginiano (Formaciones Vaca Muerta, Quintuco y Mulichinco) en el suroeste de la provincia de Neuquén. 9° Congreso Geológico Argentino, Actas, 1, 221–235.

Hampton, M.A., Lee, H.J., Locat, J. 1996. Submarine landslides. Reviews of Geophysics 34, 33–59.

Herrle, J.O., Pross, J., Friedrich, O., Hemleben, C. 2003. Short-term environmental changes in the Cretaceous Tethyan Ocean; micropalaeontological evidence from the early Albian Oceanic Anoxic Event 1b. Terra Nova 15, 14–19.

31

Kietzmann, D.A., Vennari, V.V. 2013. Sedimentología y estratigrafía de la Formación Vaca Muerta (Tithoniano-Berriasiano) en el área del cerro Domuyo, norte de Neuquén, Argentina. Andean Geology 40, 41–65.

Kietzmann, D.A., Palma, R.M., Riccardi, A.C., Martín-Chivelet, J., López-Gómez, J. 2014a. Sedimentology and sequence stratigraphy of a Tithonian–Valanginian carbonate ramp (Vaca Muerta Formation): A misunderstood exceptional source rock in the Southern Mendoza area of the Neuquén Basin, Argentina. Sedimentary Geology 302, 64–86.

Kietzmann, D.A., Ambrosio, A., Suriano, J., Alonso, S., Vennari, V.V., Aguirre-Urreta, M.B., Depine, G., Repol, D. 2014b. Variaciones de facies en las secuencias basales de la Formación Vaca Muerta en su localidad tipo (Sierra de la Vaca Muerta), Cuenca Neuquina: IAPG IX Congreso de Exploración y Desarrollo de Hidrocarburos TT2, Mendoza, Argentina, November 3–7, 2014, 299–317.

Kietzmann, D.A., Ambrosio, A.L, Suriano, J., Alonso, M.S., González Tomassini, F., Depine, G., Repol, D. 2016. The Vaca Muerta–Quintuco system (Tithonian–Valanginian) in the Neuquén Basin, Argentina: A view from the outcrops in the Chos Malal fold and thrust belt. AAPG Bulletin 100, 743–771.

Krim, N., Bonnel, C., Tribovillard, N., Imbert, P., Aubourg, Ch., Riboulleau, A., Bout-Roumazeilles, V., Hoareau, G., Fasentieux, B. 2017. Paleoenvironmental evolution of the southern Neuquèn basin (Argentina) during the Tithonian-Berriasian (Vaca Muerta and Picún Leufú Formations): a multi-proxy approach. Bulletin de la Société Géologique de France 188, https://doi.org/10.1051/bsgf/2017196.

Leanza, H.A., Wiedmann, J. 1989. Nuevos ammonites del Berriasiano/Valanginiano (Cretácico inferior) de Neuquén, Argentina. In: Wiedmann, J. (Ed.): Cretaceous of the Western Tethys. Proceedings 3rd international Cretaceous Symposium, E. Schweizerbart'sche Verlagsbuchhandlung: 793–810, Stuttgart.

Leanza, H.A., Hugo, C. 2005. Hoja Geológica 3969 - I, Zapala (escala 1: 250.000), Provincia del Neuquén, Servicio Geológico y Minero Argentino, Boletín 275, 1–136.

Leanza, H.A., Repol, D., Sruoga, P., Salvarredy Aranguren, M. 2002. Nuevas unidades estratigráficas del Mesozoico y Cenozoico en la comarca de Huncal, provincia del Neuquén, Argentina. 15º Congreso Geológico Argentino, Actas 1: 619–624.

Leanza, H.A., Hugo, C.A., Repol, D., Salvarredy Aranguren, M. 2003. Miembro Huncal (Berriasiano inferior): un episodio turbidítico en la Formación Vaca Muerta, Cuenca Neuquina, Argentina. Revista de la Asociación Geológica Argentina 58, 248–254.

Leanza, H.A., Repol, D., Hugo, C., Sruoga, P., 2006. Hoja Geológica 3769-31, Chorriaca (escala 1: 100.000), Provincia del Neuquén, Servicio Geológico y Minero Argentino, Boletín 354, 1–93.

Leanza, H.A., Sattler, F., Martinez, R.S., Carbone, O. 2011. La Formación Vaca Muerta y equivalentes (Jurásico Tardío – Cretácico Temprano) en la Cuenca Neuquina. In: Leanza, H.A., Arregui, C., Carbone, O., Danieli, J.C., Vallés, J.M. (Eds.), Geología y

Recursos Naturales de la Provincia de Neuquén. Relatorio del XVIII Congreso Geológico Argentino, Buenos Aires, pp. 113-129.

Lees, J.A., Bown, P.R., Young, J.R., Riding, J.B. 2004. Evidence for annual records of phytoplankton productivity in the Kimmeridgian Clay Formation coccolith stone bands (Upper Jurassic, Dorset, UK). Marine Micropaleontology 52, 29- 49.

Legarreta, L., Gulisano, C.A. 1989. Análisis estratigráfico secuencial de la Cuenca Neuquina (Triásico superior-Terciario inferior. In: Chebli G., Spalletti, L.A. (Eds.), Cuencas Sedimentarias Argentinas: Universidad Nacional de Tucumán Serie Correlación Geológica 6, 221–243.

Legarreta, L., Uliana, M.A. 1991. Jurassic-Cretaceous marine oscillations and geometry of back-arc basin fill, central Argentine Andes. International Association of Sedimentology, Special Publication 12, 429–450, London.

Legarreta, L., Uliana, M.A. 1996. The Jurassic succession in west-central Argentina: stratal patterns, sequences and paleogeographic evolution. Palaeogeography, Palaeoclimatology, Palaeoecology 120, 303–330.

Lescano, M., Concheyro, A. 2014. Nanocónidos del Grupo Mendoza (Cretácico Inferior) en la Provincia del Neuquén, República Argentina: Taxonomía, cronoestratigrafía e implicancias paleogeográficas. Ameghiniana 51, 466–499.

Lewis, K.B. 1971. Slumping on a continental slope inclined at $1°- 4 °$. Sedimentology 16, 97–110.

Lowe, D.R. 1982. Sediment gravity flows: II. Depositional models with special reference to the deposits of high density turbidity currents. Journal of Sedimetary Petrology 52, 279–297.

Marchese, H.G. 1971. Litoestratigrafia y variaciones faciales de las sedimentitas mesozoicas de la Cuenca Neuquina, provincia del Neuquén, República Argentina. Revista de la Asociación Geológica Argentina 26, 343–410.

Martin-Chivelet, J., Palma, R., Gómez J., Kietzmann, D. 2011. Earthquake-induced soft-sediment deformation structures in Upper Jurassic open-marine microbialites (Neuquén Basin, Argentina). Sedimentary Geology 235, 210–221.

Melinte, M., Mutterlose, J. 2001. A Valanginian (Early Cretaceous) "Boreal nannoplankton excursion" in sections from Romania. Marine Micropaleontology 43, 1–25.

Mitchum, R.M., Uliana, M.A. 1985. Seismic stratigraphy of carbonate depositional sequences, Upper Jurassic-Lower Cretaceous. Neuquén Basin, Argentina. In: Berg, R.B., Woolverton, D.G. (Eds.), Seismic stratigraphy: An integrated approach to hydrocarbon exploration, AAPG Memoir 39, 255–274.

Mosquera, A., Ramos, V.A. 2006. Intraplate deformation in the Neuquén Embayment. In: Kay, S.M., Ramos, V.A. (Eds.), Evolution of an Andean margin: A tectonic and

magmatic view from the Andes to the Neuquén Basin (35°-39°S lat). Geological Society of America Special Paper 407, 97–123.

Mutterlose, J. 1991. Das Verteilungs- und Migrationsmuster des kalkigen Nannoplanktons in der borealen Unter-Kreide (Valangin- Apt) NW-Deutschlands. Palaeontographica B221, 27–152.

Mutterlose, J. 1992. Biostratigraphy and palaeobiogeography of Early Cretaceous calcareous nannofossils. Cretaceous Research 13, 167–189.

Mutterlose, J., Bornemann, A., Herrle, J. 2005. Mesozoic calcareous nannofossils - state of the art. Paläontologische Zeitschrift 79, 113–133.

Mutti, E., Tinterri, R., Remacha, E., Mavilla, N., Angella, S., Fava, L. 1999. An introduction to the analysis of ancient turbidite basins from an outcrop perspective. American Association of Petroleum Geologists, Continuing Education Course Notes Series 39. Oklahoma, USA.

Naipauer, M., Ramos, V.A. 2016. Changes in source areas at Neuquén Basin: Mesozoic evolution and tectonic setting based on U-Pb ages on zircons. In: Folguera, A., Naipauer, M., Sagripanti, L., Ghiglione, M., Orts, D. (Eds.), Growth of the Southern Andes, Springer, pp. 33-61.

Naipauer, M., García Morabito, E., Marques, J.C., Tunik, V., Rojas Vera, E., Vujovich, G.I., Pimentel, M.P., Ramos, V.A. 2012. Intraplate Late Jurassic deformation and exhumation in western central Argentina: Constraints from surface data and U-Pb detrital zircon ages. Tectonophysics 524-525, 59–75.

Naipauer, M., Tunik, M., Marques, J.C., Rojas Vera, E.A., Vujovich, G.I., Pimentel, M.M., Ramos, V.A. 2015. U-Pb detrital zircon ages of Upper Jurassic continental successions: implications for the provenance and absolute age of the Jurassic-Cretaceous boundary in the Neuquén Basin. In: Sepúlveda, S., Giambiagi, L., Pinto, L., Moreiras, S., Tunik, M., Hoke, G., Farías, M. (Eds.), Geodynamic Processes in the Andes of Central Chile and Argentina. Geological Society, Special Publications 399,131–154.

Naipauer, M., García Morabito, E., Manassero, M., Valencia, V.A., Ramos, V.A. 2018. Volcanic arc or intraplate magmatic input? A provenance analysis from the Lower Jurassic units of the Neuquén basin. In: Folguera, A., Contreras Reyes, E., Heredia, N., Encinas, A., Oliveros, V., Dávila, F., Collo, G., Giambiagi, L., Naipauer, M., Maksymowicz, A., Alvarez, O. (Eds.), The evolution of the Chilean-Argentinean Andes. Springer, pp. 191-222.

Ogg, J.G., Agterberg, F.P., Gradstein, F.M. 2004. The Cretaceous Period. In: Gradstein, F., Ogg, J.G., Smith, A. (eds.), A Geologic Time Scale. Cambridge University Press, Cambridge, pp. 344-383.

Pángaro, F., Pereira, D.M., Micucci, E. 2009. El sinrift de la Dorsal de Huincul, Cuenca Neuquina: evolución y control sobre la estratigrafía y estructura del área. Revista de la Asociación Geológica Argentina 65, 265–277.

Pankhurst, R.J., Rapela, C.W., Fanning, C.M., Márquez, M. 2006. Gondwanide continental collision and the origin of Patagonia. Earth-Science Reviews 76, 235–257.

Pankhurst, R.J., Rapela, C.W., López de Luchi,M.G., Rapalini, A.E., Fanning, C.M., Galindo, C. 2014. The Gondwana connections of northern Patagonia. Journal of the Geological Society 171, 313–328.

Pittet, B., Mattioli, E. 2002. The carbonate signal and calcareous nannofossil distribution in an upper Jurassic section (Balingen- Tieringen, Late Oxfordian, southern Germany). Palaeogeography, Palaeoclimatology, Palaeoecology 179, 71–96.

Pose, F., Gangui A., Galeazzi, S. 2014. Estratigrafía secuencial del intervalo Quintuco-Vaca Muerta en el Engolfamiento Neuquino, Cuenca Neuquina, Argentina. 9º Congreso de Exploración y desarrollo de hidrocarburos, Simposio de recursos no convencionales: Ampliando el horizonte energético, 211–229.

Premoli Silva, I., Erba, E., Tornaghi, M.E. 1989. Paleoenvironmental signals and changes in surface fertility in Mid Cretaceous C org-rich pelagic facies of the Fucoid Marls (Central Italy). Geobios, Memoir Special 11, 225–236.

Ramos, V.A. 1988. The tectonics of the Central Andes: 30° to 33° S latitude. In: Clark, S., Burchfiel, D. (Eds.), Processes in Continental Lithospheric Deformation, Geological Society of América, Special Paper 218, 31–54, Boulder.

Reijenstein, H., Lanusse, I., Oviedo, P., Licitra, D., Sotelo, D., Vittore, F., Quiroga, J., González Tomassini, F. 2017 ¿Deslizamientos en Vaca Muerta? Observaciones e integración de datos sísmicos, pozos y coronas en el yacimiento Loma Campana, Cuenca Neuquina, Argentina. 10º Congreso Geológico Argentino, Simposio 5: Geología de la Formación Vaca Muerta, 122-129, San Miguel de Tucumán.

Rossel, R., Oliveros, V., Mescua, J., Tapia, F., Ducea, M.N., Calderón, S., Charrier, R., Hoffman, D. 2014. The Upper Jurassic volcanism of the Río Damas-Tordillo Formation (33°- 35.5°S): Insights on petrogenesis, chronology, provenance and tectonic implications. Andean Geology 41, 529-557.

Roth, P., Krumbach, K. 1986. Middle Cretaceous Calcareous Nannofossil Biogeography and Preservation in the Atlantic and Indian Oceans: Implications for Palaeoceanography. Marine Micropalaeontology 10, 235–266.

Santiago, M.F., Rauzi, R.S., Laffitte, G.A., Alvarado, O.A. 2014. La Formación Vaca Muerta como objetivo exploratorio no convencional en la subcuenca de Picún Leufú, Neuquén, Argentina. 9º Congreso de Exploración y Desarrollo de Hidrocarburos, Simposio de recursos no convencionales: Ampliando el horizonte energético, 275–314.

Scasso, R.A., Alonso, M.S., Lanes, S., Villar, H.J., Laffitte, G. 2005. Geochemistry and petrology of a Middle Tithonian limestone-marl rhythmite in the Neuquen Basin, Argentina: depositional and burial history. In: Veiga, G.D., Spalletti, L.A., Howell, J.A., Schwarz, E. (Eds.), The Neuquen Basin, Argentina: A case study in sequence

stratigraphy and Basin Dynamics. Geological Society, London, Special Publication 252, 207–229.

Spalletti, L., Franzese, J., Matheos, S., Schwarz, E. 2000. Sequence stratigraphy of a tidally-dominated carbonate-siliciclastic ramp; the Tithonian of the southern Neuquén Basin, Argentina. Journal of the Geological Society 157, 433–446.

Spalletti, L.A., Veiga, G.D., Schwarz, E., Franzese, F. 2008. Depósitos de flujos gravitacionales subácueos de sedimentos en el flanco activo de la cuenca Neuquina durante el Cretácico Temprano. Revista de la Asociación Geológica Argentina 63, 442 – 453.

Spalletti, L.A., Schwarz, E., Veiga, G.D. 2014. Geoquímica inorgánica como indicador de procedencia y ambiente sedimentario en sucesiones de lutitas negras: los depósitos transgresivos titonianos (Formación Vaca Muerta) de la Cuenca Neuquina, Argentina. Andean Geology 41, 401–435.

Street, C., Bown, P. 2000. Palaeobiogeography of Early Cretaceous (Berriasian-Barremian) calcareous nannoplankton. Marine Micropalaeontology 39, 265–291.

Talling, P.J., Masson, D.G., Sumner, E.J., Malgesini, G. 2012. Subaqueous sediment density flows: depositional processes and deposit types. Sedimentology 59, 1937–2003.

Tunik, M.A., Folguera, A., Naipauer, M., Pimentel, M., Ramos, V.A. 2010. Early uplift and orogenic deformation in the Neuquén Basin: Constraints on the Andean uplift from U–Pb and Hf isotopic data of detrital zircons. Tectonophysics 489, 258–273.

Uliana, M.A., Legarreta, L. 1993. Hydrocarbons habitat in a Triassic-to-Cretaceous sub-Andean setting: Neuquén basin, Argentina. Journal of Petroleum Geologists 16, 397–420.

Urlaub, M., Talling, P.J., Masson, D.G. 2013. Timing and frequency of large submarine landslides: implications for understanding triggers and future geohazard. Quaternary Science Reviews 72, 63–82.

Vennari, V.V., Lescano, M., Naipauer, M., Aguirre-Urreta, M.B., Concheyro, A., Schaltegger, U., Armstrong, R., Pimentel, M., Ramos, V.A. 2014. New constraints on the Jurassic–Cretaceous boundary in the High Andes using high-precision U-Pb data. Gondwana Research 26, 374–385.

Vergani, G.D., Tankard, A.J., Belotti, H.J., Welsink, H.J. 1995. Tectonic evolution and paleogeography of the Neuquén Basin Argentina. In: Tankard, A.J., Suárez, R., Welsink, H.J. (Eds.), Petroleum Basins of South America. American Association of Petroleum Geologists, Memoir 62, 383-402.

Weaver, C.E. 1931. Paleontology of the Jurassic and Cretaceous of West Central Argentina. Memoir University of Washington 1, 1–469.

Williams, J., Bralower, T. 1995. Nannofossil assemblages, fine fraction stable isotopes, and the paleoceanography of the Valanginian- Barremian (Early Cretaceous) North Sea Basin. Paleoceanography 10, 815–839.

Worden, R.H., Morad, S. 2003. Clay minerals in sandstones: controls on formation, distribution and evolution. In: Worden, R.H., Morad, S. (Eds.), Clay Mineral Cements in Sandstones. International Association of Sedimentologists, Special Publication 34, 3–41.

Zamora Valcarce, G., Zapata, T., Del Pino, D., Ansa, A., 2006. Structural evolution and magmatic characteristics of the Agrio Fold-and-thrust belt. In: Kay, S.M., Ramos, V.A. (Eds.), Evolution of an Andean margin: a tectonic and magmatic view from the Andes to the Neuquén Basin (35°–39° lat). Geological Society of America, Special Paper 407, 125–145.

SUPPLEMENTARY MATERIAL

Table 1 of the Supplementary material: section C

BAFC-NP	meters	*W. fossacincta*	*W. barnesiae*	*Micrantholithus sp.*	*M. hozchulzii*	*M. obtusus*	*Z. embergerii*	*W. biporta*	*U. granulosa*	*E. primus*	*Staurolithites sp.*	*Z. xenotus*	*R. asper*	*cocosfera*	*C. cuvillieri*	*D. lehmanii*	*T. gabalus*	*E. gallicus*	*C. margerelli*	*Z. howeii*	*M. pemmatoidea*	*E. hauterivianus*	*R. surirella*	*Zeugrahbdothus sp.*	*T. stradneri*	*H. chiastia*
3979																										
3978	98.0						0.3												0.3				0.3			1.0
3977		38.8	5.6		53.1	0.6							0.6								0.6		0.6			
3976		64.7	29.4																						5.9	
3975		100																								
3974																										
3973																										
3972		87.5	12.5																							
3971																										
3970																										
3969																										
3968		74.6	19.3	0.9	1.8	1.8		1.8																		
3967																										
3966																										
3965																										
3964		58.4	18.3	3.7	11.2	2.9	0.5		0.5				2.1			0.5			0.5		0.5		0.5	0.5		
3963		70.8			29.2																					
3962		87.4	7.6	1.0	0.2	0.6		1.5	0.6									0.4	0.4				0.3			
3961																										
3960		91.2	1.2		3.2	0.7	0.5		0.4				1.8					0.3		0.4	0.3					
3959		63.0	32.8	1.0	0.6			1.0	0.6										1.0							

3958															
3957	87.9	4.9	0.5	2.7	0.5	0.5					0.5	0.5	0.5	0.5	0.5
3956	83.1	1.7	2.4	10.7	0.3	1.7									
3955	69.4	9.5	2.9	13.5	0.9	0.5	0.5	0.5	0.8	0.5	0.5	0.5			

Table 2 of the Supplementary material, section B

BAFC-NP	meters	*W. fossacincta*	*M. hozchulzii*	*W. barnesiae*	*M. obtusus*	*Z. embergerii*	*D. lehmanii*	*M. pemmatoidea*	*H. chiastia*
4139									
4138		56.8	2.9	40.3					
4137		53.8	3.9	26.8	3.9	3.9	7.7		
4136		25.0	52.0	3.6	7.0		7.0	3.6	1.8
4135									
4134									
4133		43.5		43.5					
4132									
4131									
4130									
4129		77.5		22.5					
4128									
4127									
4126									
4125		98.0	2.0						
4124									

Table 3 of the Supplementary material, section D

BAFC-NP	meters	*W. fossacincta*	*W. barnesiae*	*M. hozchulzii*	*M. obtusus*	*Z. embergerii*	*E. hauterivianus*
4146		82.5		10.3	7.2		
4145		75.7	22.5			1.8	
4144							
4143							
4142							
4141			100.0				
4140		58.4	37.4	3.2		0.5	0.5

Table 4 of the Supplementary material, petrographic data

SAMPLE	Qtz m	Qtz p	Plg	Kfs	Lv	Ls	Lpyr	Lp/m	Mi	CCar	Cqtz	CChl	COx	Ma
pnh-5	39.15	3.18	23.61	3.23	19.63	0.30			2.00	0.50	0.70	3.50	1.50	2.70
pnh-4	32.15	4.48	26.94	4.97	16.31	2.17			1.60	4.33	0.50	2.80		3.75
pnh-3	35.42	4.32	22.33	3.07	19.23	1.42			1.30	6.03	1.12	1.67	1.20	2.89
pnh-2	46.26	3.12	18.43	3.11	15.19	1.18			1.28	6.19	1.20	1.15	1.20	1.69
pnh-1	41.31	3.82	24.14	4.38	14.22	1.35			1.18	1.12	1.41	4.09	1.11	1.87
lsh-2	36.41	3.12	24.11	4.52	26.11	0.31			1.00			1.15	2.10	1.17
lsh-1	34.55	3.02	24.66	4.12	18.72	3.13	0.80		1.25	2.15		2.19		5.41
H2-S1	33.11	1.92	30.51	4.11	17.19	1.12	0.75		1.18	2.25	1.41	2.15	2.15	2.15
VM1-M6	44.96	2.11	15.82	5.63	18.31	2.13			1.01	5.12	2.12	1.02	0.45	1.32
HSE-3	46.25	1.87	21.08	1.18	15.69	1.25		1.74	1.25	4.41	1.13	0.82	1.15	2.18
HSE-2	45.65	3.21	24.61	3.27	10.75	2.13			2.14	1.24		1.71	1.12	4.17
HSE-1	29.49	4.83	24.00	4.50	24.29			1.25	2.11	1.32	0.71	1.14	1.15	5.21

U-Pb Analytical methods

Sample VM-01 (Laboratório de Geocronologia, Instituto de Geociências da Universidade de Brasília, Brasil):

The zircon grains were radon selected and set in epoxy resin mounts. The mount surface was polished to expose the grain interiors. Backscattered electron images of zircons were obtained using an SEM JEOL JSM 5800 at Universidade de Brasilia (UnB), Brazil. The samples were loaded into a New Wave UP213 Nd:YAG laser (λ=213 nm), linked to a Thermo Finnigan Neptune Multi-collector ICPMS. Helium was used as the carrier gas and mixed with argon before entering the ICP. The laser was run at a frequency of 10 Hz and energy of 34% and the diameter with a spot size of 30 µm. Laser induced fractionation of the 206Pb/238U ratio was corrected using the linear regression method (Kosler et al., 2002). Two international zircon standards were analyzed throughout the U-Pb analyses. The zircon standard GJ-1 (Jackson et al, 2004) was used as the primary standard in a standard-sample bracketing method, accounting for mass bias and drift correction. The resulting correction factor for each sample analysis considers the relative position of each analysis within the sequence of 4 samples bracketed by two standard and two blank analyses each (Albarède et al, 2004). Analyses were performed using spot size of 30 µm. The Temora 2 standard (Black et al, 2004) was run at the start and the end of each analytical session, yielding accuracy around 2% and precision in the range of 1 %. The errors of sample analyses were propagated by quadratic addition of the external uncertainty observed for the standards to the reproducibility and within-run precision of each unknown analysis. The instrumental set-up and further details of the analytical method applied are given by Buhn et al (2009). Masses 204, 206 and 207 were measured with ion counters, and

39

238U was analyzed on a Faraday cup. 202Hg signal was monitored by an ion counter for correction of the isobaric interference between 204Hg and 204Pb. The signals during ablation were taken in 40 cycles of 1 sec each. For data evaluation, only coherent intervals of signal response were considered. Data reduction was performed with an in-house Excel spreadsheet, which considers blank values, zircon standards composition and errors, and error propagation. The 204Pb signal intensity was calculated and corrected using a natural 202Hg/204Hg ratio of 4.346. Common Pb correction was applied for zircons with 206Pb/204Pb lower than 1000, applying the common lead composition following the Stacey and Kramers (1975) model. Plotting of U-Pb data was performed using ISOPLOT v.3 (Ludwig, 2003) and errors for isotopic ratios are presented at the 2σ level. Because of the statistical treatment applied in calculating Concordia Ages, those are more precise than any individual U-Pb or Pb-Pb ages (Ludwig, 2003) and, in the present study, always correspond to less than the 2% accuracy obtained from the intercalibration of the standards. Consequently, the Isoplot calculated errors were modified in order to incorporate this uncertainty level and, hence, represent a more realistic age in terms of the analytical limitations of the method. The age probability plots (Ludwig, 2003) used in this study were constructed using the 206Pb/238U age for young (<1.0 Ga) zircons and the 206Pb/207Pb age for older (>1.0 Ga) grains

REFERENCES

Albarede, F., Telouk, P., Blichert-Toft, J., Boyet, M., Agranier, A. and Nelson, B. 2004. Precise and accurate isotopic measurements using multiple-collector ICPMS. Geochimica et Cosmochimica Acta, 68 (12), 2725-2744.

Black, L.P., Kamo, S.L., Allen, C.M., Davis, D.W., Aleinikoff, J.N., Valley, J.W., Mundil, R., Campbell, I.H., Korsch, R.J., Williams, I.S., and Foudoulis, C., 2004. Improved 206Pb/238U microprobe geochronology by the monitoring of a trace-element-related matrix effect; SHRIMP, ID-TIMS, ELA-ICP-MS and oxygen isotope documentation for a series of zircon standards: Chemical Geology, 205, 115-140.

Buhn, B., Pimentel, M.M., Matteini, M. and Dantas, E. 2009. High spatial resolution analysis of Pb and U isotopes for geochronology by laser ablation multi-collector inductively coupled plasma mass spectrometry (LA-MC-ICP-MS). Anais da Academia Brasileira de Ciências, 81, 99-114.

Jackson, S.E., Pearson, N.J., Griffin, W.L., Belousova, E.A. 2004. The application of laser ablation-inductively coupled plasma-mass spectrometry to in situ U–Pb zircon geochronology. Chemical Geology, 211, 47-69.

Košler, J., Fonneland, H., Sylvester, P., Tubrett, M., Pedersen, R.B. 2002. U–Pb dating of detrital zircons for sediment provenance studies–a comparison of laser ablation ICP-MS and SIMS techniques. Chemical Geology, 182, 605-618.

Ludwig, K.R. 2003. Isoplot 3.00: A geochronological toolkit for Microsoft Excel. Berkeley Geochronological Center, Special Publication, 4, 70p.

Stacey, J.S. and Kramers, J.D. 1975. Approximation of terrestrial lead isotope evolution by a two-stage model. Earth and Planetary Science Letters, 26, 207-221.

Table 5 of the Supplementary material, U-Pb data

Summary of analytical results by MC-ICPMS-LA U-Pb zircons data.
Data analyzed in the Universidade de Brasilia (UnB), Brazil
SAMPLE VM-01 - Huncal Member (GPS: 37º59´36,6´´ S - 70º25´56,9´´ N)

Spot	f(206)	Th/U	6/4.	7/6.	1s	7/5.	1s	6/8.	1s	Rho	7/6.	1s	7/5.	1s	6/8.	1s	Conc	Conc
	%		ratio	ratio	(%)	ratio	(%)	ratio	(%)		age	(%)	age	(%)	age	(%)	(%)	(%)*
010-Z05B	0.05	0.35	40334.4	0.05	0.66	0.15	1.18	0.02	0.97	0.81	170	16	144	2	139	1	81	96
078-Z50B	0.06	0.35	17146.9	0.05	0.75	0.15	1.00	0.02	0.67	0.62	71	18	144	1	144	1	202	100
069-Z45N	0.09	0.44	20664.1	0.05	0.68	0.16	0.95	0.02	0.67	0.65	157	16	149	1	144	1	92	97
077-Z50N	0.08	0.27	22589.5	0.05	0.75	0.15	1.12	0.02	0.83	0.71	53	18	144	2	145	1	272	101
067-Z43	0.20	1.02	9390.5	0.05	0.82	0.18	1.07	0.03	0.68	0.59	38	20	168	2	173	1	456	103
088-Z57	0.03	0.37	47104.3	0.05	0.64	0.19	1.06	0.03	0.84	0.77	120	16	174	2	173	1	144	99
076-Z49	0.06	1.10	31074.9	0.05	0.67	0.19	0.92	0.03	0.62	0.63	128	16	175	1	174	1	136	99
028-Z16B	0.22	0.72	5208.8	0.05	1.19	0.19	1.44	0.03	0.82	0.54	103	29	174	2	174	1	168	100
058-Z37	0.17	0.31	18443.9	0.05	0.60	0.19	0.83	0.03	0.57	0.63	48	15	172	1	177	1	370	102
016-Z09	0.35	0.84	5295.3	0.05	1.17	0.19	1.44	0.03	0.84	0.55	49	29	174	2	178	1	367	102
046-Z29	0.03	1.03	55958.2	0.05	0.73	0.20	1.04	0.03	0.74	0.67	131	18	181	2	180	1	137	99
074-Z47	0.08	0.32	11084.2	0.05	0.89	0.20	1.11	0.03	0.67	0.55	170	21	185	2	181	1	106	98
073-Z46	0.04	0.96	50334.5	0.05	0.56	0.19	0.94	0.03	0.75	0.78	104	14	180	2	181	1	174	100
023-Z13B	0.09	0.48	21163.3	0.05	1.05	0.18	1.30	0.03	0.77	0.56	-47	26	170	2	181	1	-381	106
075-Z48	0.03	0.20	70076.1	0.05	0.60	0.20	0.88	0.03	0.64	0.68	168	15	185	1	181	1	107	98
085-Z54	0.32	1.04	5678.7	0.05	0.82	0.20	1.11	0.03	0.75	0.64	192	20	187	2	182	1	95	97
030-Z18	0.07	0.99	25597.4	0.05	0.93	0.20	1.15	0.03	0.67	0.53	125	23	184	2	184	1	147	100
086-Z55	0.07	1.26	27347.9	0.05	0.55	0.20	1.03	0.03	0.87	0.83	89	13	183	2	186	2	209	101
037-Z22	0.05	0.43	39899.3	0.05	0.64	0.21	0.97	0.03	0.74	0.73	115	15	191	2	192	1	167	100
065-Z41	0.11	0.75	16275.2	0.05	1.05	0.22	1.33	0.03	0.82	0.58	142	25	199	2	198	2	140	100
079-Z51	0.06	0.90	30341.5	0.05	0.63	0.23	0.92	0.03	0.67	0.69	199	15	211	2	206	1	103	98
019-Z12	0.03	0.66	61162.5	0.05	0.74	0.24	1.03	0.04	0.72	0.66	122	18	222	2	225	2	184	101
053-Z33	0.18	0.53	10001.4	0.05	0.61	0.24	0.92	0.04	0.69	0.71	119	15	222	2	225	2	189	102
038-Z23	0.02	0.52	90284.9	0.05	0.54	0.27	0.79	0.04	0.58	0.67	248	13	241	2	233	1	94	97
045-Z28	0.07	0.45	26071.6	0.05	0.67	0.26	1.09	0.04	0.86	0.77	168	16	235	2	235	2	140	100
064-Z40	0.05	0.50	50630.6	0.05	0.52	0.27	1.22	0.04	1.10	0.90	159	12	239	3	240	3	151	101
005-Z02N	0.01	0.74	172959.9	0.05	0.52	0.29	0.91	0.04	0.75	0.80	272	12	260	2	252	2	93	97
006-Z02B	0.02	0.73	112250.1	0.05	0.37	0.28	0.86	0.04	0.77	0.88	158	9	251	2	254	2	160	101
090-Z59	0.05	0.48	34506.5	0.05	0.87	0.29	1.12	0.04	0.70	0.59	142	21	258	3	263	2	185	102
039-Z24	0.02	0.59	86163.7	0.05	0.41	0.30	1.06	0.04	0.98	0.92	226	10	268	3	265	3	117	99
089-Z58	0.02	0.37	93254.4	0.05	0.57	0.30	1.52	0.04	1.41	0.92	190	14	268	4	269	4	141	100
008-Z04	0.02	0.25	16868.2	0.05	0.49	0.32	0.86	0.04	0.70	0.79	295	11	282	2	272	2	92	97
087-Z56	0.01	0.44	250305.5	0.05	0.48	0.31	0.71	0.04	0.52	0.65	192	12	275	2	277	1	144	101
040-Z25	0.00	0.50	534739.0	0.05	0.54	0.31	0.89	0.04	0.70	0.76	161	13	272	2	278	2	173	102

048-Z30B	0.14	0.10	36390.5	0.05	0.87	0.32	1.16	0.04	0.78	0.63	265	20	284	3	**279**	**2**	105	**98**
060-Z39	0.06	0.43	29212.5	0.05	0.68	0.32	1.06	0.04	0.81	0.74	249	16	283	3	**279**	**2**	112	**99**
035-Z20	0.08	0.26	22574.3	0.05	0.49	0.34	0.88	0.04	0.74	0.81	328	11	295	2	**282**	**2**	86	**96**
018-Z11	0.03	0.34	33266.5	0.05	0.56	0.33	0.83	0.05	0.61	0.69	224	13	288	2	**287**	**2**	128	**100**
013-Z06	0.02	0.52	98863.5	0.05	0.43	0.34	0.89	0.05	0.78	0.86	280	10	295	2	**289**	**2**	103	**98**
056-Z35	0.11	1.48	16106.2	0.05	0.84	0.38	1.04	0.05	0.61	0.53	270	20	324	3	**323**	**2**	119	**100**
025-Z15N	0.03	0.25	56793.6	0.06	0.86	0.42	1.19	0.05	0.82	0.66	406	20	353	4	**336**	**3**	83	**95**
004-Z01	0.03	0.36	48436.37	0.05	0.76	0.43	1.15	0.06	0.86	0.73	338	18	365	4	**359**	**3**	106	**98**
026-Z15B	0.08	0.20	23506.97	0.05	0.54	0.44	0.95	0.06	0.79	0.80	294	13	373	3	**376**	**3**	128	**101**
049-Z31	0.05	0.29	37786.62	0.05	0.37	0.46	0.72	0.06	0.62	0.82	239	9	387	2	**401**	**2**	167	**104**
036-Z21	0.06	0.24	27909.24	0.05	0.41	0.48	0.72	0.07	0.59	0.77	277	10	397	2	**407**	**2**	147	**102**
007-Z03	0.03	0.95	52574.08	0.06	0.59	0.55	1.13	0.07	0.96	0.84	409	14	448	4	**443**	**4**	108	**99**
068-Z44	0.01	0.13	212653.9	0.06	0.31	0.67	1.47	0.08	1.44	0.98	541	7	523	6	**505**	**7**	93	**97**
016-Z68	0.03	0.45	68521.88	0.05	0.42	0.16	1.69	0.02	1.63	0.97	25	10	148	2	**151**	**2**	612	**102**
017-Z69	0.03	0.39	56715.93	0.05	0.50	0.16	1.39	0.02	1.30	0.93	79	12	152	2	**152**	**2**	193	**100**
015-Z67	0.16	0.36	11297.05	0.05	0.72	0.16	2.09	0.02	1.96	0.94	19	18	149	3	**153**	**3**	811	**103**
047-Z88	0.14	1.04	12812.61	0.05	1.35	0.18	1.70	0.03	1.02	0.58	142	33	171	3	**168**	**2**	118	**98**
048-Z89	0.06	0.46	29421.94	0.05	0.84	0.18	1.17	0.03	0.82	0.67	72	21	170	2	**172**	**1**	237	**101**
030-Z78	0.05	1.05	40315.67	0.05	0.52	0.18	1.12	0.03	1.00	0.88	20	13	168	2	**174**	**2**	865	**103**
034-Z79	0.06	0.71	42848.81	0.05	0.48	0.18	0.89	0.03	0.75	0.82	50	12	170	1	**174**	**1**	350	**102**
004-Z60	0.05	0.24	24259.35	0.05	0.76	0.19	1.35	0.03	1.11	0.82	123	18	177	2	**177**	**2**	143	**99**
028-Z76	0.04	0.80	20884.23	0.05	0.69	0.19	1.10	0.03	0.85	0.76	102	17	180	2	**181**	**2**	178	**100**
042-Z85	0.18	0.57	10427.78	0.05	1.54	0.21	1.92	0.03	1.15	0.58	235	37	190	3	**181**	**2**	77	**95**
036-Z81	0.08	1.12	22204.99	0.05	0.76	0.20	1.22	0.03	0.96	0.77	82	18	183	2	**186**	**2**	225	**101**
039-Z82	0.05	0.29	36523.71	0.05	0.57	0.20	1.00	0.03	0.82	0.80	48	14	184	2	**190**	**2**	398	**103**
021-Z71	0.06	0.68	30702.74	0.05	1.66	0.22	2.02	0.03	1.15	0.56	254	39	200	4	**190**	**2**	75	**95**
011-Z65	0.09	0.72	20651.48	0.05	0.51	0.22	1.62	0.03	1.54	0.95	51	12	202	3	**209**	**3**	410	**104**
027-Z75	0.06	0.84	31664.34	0.05	0.72	0.24	1.18	0.03	0.93	0.77	123	18	215	2	**217**	**2**	176	**101**
012-Z66	0.11	0.80	15961.44	0.05	0.79	0.25	1.86	0.04	1.69	0.90	144	19	228	4	**230**	**4**	160	**101**
054-Z92	0.03	0.63	68034.50	0.05	0.42	0.27	1.25	0.04	1.18	0.94	104	10	243	3	**250**	**3**	240	**103**
041-Z84	0.04	0.67	50603.41	0.05	0.55	0.29	0.94	0.04	0.76	0.78	217	13	259	2	**256**	**2**	118	**99**
018-Z70	0.01	0.10	227017.5	0.05	0.31	0.31	1.21	0.04	1.16	0.96	220	7	274	3	**273**	**3**	124	**100**
023-Z73	0.01	0.10	173254.5	0.05	0.31	0.32	1.31	0.05	1.28	0.97	197	8	282	3	**284**	**4**	145	**101**
053-Z91	0.04	0.30	49918.54	0.05	0.91	0.32	1.45	0.05	1.13	0.77	129	22	279	4	**289**	**3**	224	**104**
005-Z61	0.04	0.44	40889.30	0.05	0.63	0.35	1.30	0.05	1.14	0.87	206	15	301	3	**305**	**3**	148	**101**
024-Z74	0.01	0.14	196514.7	0.05	0.46	0.40	1.11	0.06	1.01	0.90	237	11	345	3	**352**	**3**	149	**102**
045-Z86	0.03	0.18	55510.24	0.05	0.54	0.47	1.16	0.06	1.03	0.88	331	12	390	4	**389**	**4**	117	**100**
010-Z64	0.07	0.24	39914.89	0.08	0.49	2.22	1.53	0.19	1.45	0.95	**1229**	**10**	1188	11	1136	15	92	**96**
Rejected analysis						-	-	-	-	-								
015-Z08	0.24	0.50	7835.84	0.05	1.30	0.12	1.84	0.02	1.29	0.69	156	31	118	2	113	1	72	96
055-Z34B	0.07	0.42	26193.10	0.05	0.59	0.14	1.09	0.02	0.92	0.82	90	14	131	1	130	1	143	99
054-Z34N	0.33	0.45	12188.27	0.05	0.77	0.14	1.01	0.02	0.65	0.59	-13	19	131	1	135	1	-1062	103
070-Z45B	0.20	0.0	9114.98	0.06	1.04	0.21	1.29	0.02	0.77	0.56	699	23	193	2	150	1	21	78
044-Z27	1.93	0.00	2567.98	0.03	1.89	0.12	2.09	0.03	0.89	0.54	-993	55	114	2	167	1	-17	147
059-Z38	0.58	1.48	3185.94	0.04	0.91	0.17	1.15	0.03	0.70	0.60	-167	23	161	2	179	1	-107	111
083-Z53N	0.07	1.10	25417.09	0.05	1.32	0.21	1.55	0.03	0.82	0.49	262	31	190	3	179	1	68	94

050-Z32	0.11	1.52	16948.24	0.05	1.38	0.20	1.53	0.03	0.66	0.39	150	33	187	3	184	1	123	99
024-Z14	0.37	0.71	4700.20	0.05	1.58	0.21	1.75	0.03	0.76	0.42	203	36	196	3	190	1	93	97
057-Z36	0.55	0.53	3349.80	0.05	2.89	0.31	3.12	0.04	1.19	0.39	306	64	274	7	263	3	86	96
066-Z42	0.07	0.29	26976.66	0.05	1.00	0.33	1.16	0.04	0.59	0.45	335	23	289	3	276	2	82	95
029-Z17	0.10	0.11	18768.25	0.07	1.23	0.81	2.24	0.09	1.87	0.83	783	27	602	10	540	10	69	90
043-Z26	0.01	0.20	118100.7	0.11	0.32	2.30	0.89	0.15	0.83	0.93	1740	6	1211	6	913	7	52	75
006-Z62	0.11	1.53	17179.18	0.04	1.50	0.17	1.91	0.03	1.18	0.60	-157	38	162	3	180	2	-114	111
022-Z72	0.15	0.90	33795.69	0.14	7.76	0.74	7.86	0.04	1.30	0.16	2154	139	560	34	245	3	11	44
029-Z77	0.13	1.10	14033.99	0.04	3.27	0.16	3.46	0.03	1.14	0.32	487.1	89.3	153.5	4.9	192	2	-39	125
035-Z80	0.07	0.34	25860.48	0.05	0.97	0.16	1.26	0.02	0.80	0.60	-49.8	24.3	150.7	1.8	159	1	-320	106
040-Z83	0.14	0.54	18153.58	0.05	2.59	0.34	2.95	0.05	1.40	0.47	229.3	61.6	294.0	7.5	294	4	128	100
046-Z87	0.07	1.30	38748.05	0.05	3.94	0.16	4.05	0.02	0.94	0.22	100.7	96.0	154.2	5.8	153	1	152	99
052-Z90	0.10	0.12	34434.97	0.06	1.12	0.35	1.80	0.05	1.42	0.78	395.7	25.8	308.0	4.8	288	4	73	94

Conc (%): 6/8 - 7/6
Conc (%)*: 6/8 - 7/5

Highlights

The age of the Huncal sandstones is late Berriasian in their type locality.

The sedimentary provenance is from the North Patagonian Massif and the Huincul High.

Sandstones and slump structures are present throughout the entire basin from the Tithonian to the Valanginian

The Huncal Member is a diachronic lithostratigraphic unit.

Author Contribution Statement

Maximiliano Naipauer: Conceptualization, Investigation, Methodology, Writing & editing, Resources, Funding acquisition

Marcos Comerio: Conceptualization, Investigation, Writing & editing

Marina Lescano: Investigation, Writing & editing

Veronica Vennari: Investigation, Writing & editing

Beatriz Aguirre-Urreta: Conceptualization, Investigation, Methodology, Writing & editing, Supervision, Funding acquisition

Marcio Pimentel: Resources, Conceptualization, Methodology, Investigation, Supervision, Funding acquisition

Victor Ramos: Conceptualization, Investigation, Methodology, Writing & editing, Supervision, Funding acquisition

Declaration of interests

☒ The authors declare that they have no known competing financial interests or personal relationships that could have appeared to influence the work reported in this paper.

☐The authors declare the following financial interests/personal relationships which may be considered as potential competing interests: